

# Randomized Channel Sparsifying Hybrid Precoding for FDD Massive MIMO Systems

1

Chang Tian\*, An Liu<sup>†</sup>, Mahdi Barzegar Khalilsarai<sup>‡</sup>, Giuseppe Caire<sup>‡</sup>, Wu Luo\*,  
and Minjian Zhao<sup>†</sup>

## Abstract

We propose a novel randomized channel sparsifying hybrid precoding (RCSHP) design to reduce the signaling overhead of channel estimation at the base station (BS) and reduce the hardware cost and power consumption at the BS in order to fully harvest benefits of frequency division duplex (FDD) massive multiple-input multiple-output (MIMO) systems. RCSHP allows time-sharing between multiple analog precoders, each serving a compatible user group. The analog precoder is adapted to the channel statistics to properly sparsify the channel for the associated user group, such that the resulting effective channel not only has enough spatial degrees of freedom (DoF) to serve this group of users, but also can be accurately estimated under the limited pilot budget. The digital precoder is adapted to the effective channel based on the duality theory to facilitate the power allocation and exploit the spatial multiplexing gain in RCSHP. We formulate the joint optimization of time-sharing factors and the associated sets of analog precoders and power allocations as a general utility optimization problem, which considers the impact of effective channel estimation error on the system performance. Then we propose an efficient stochastic successive convex approximation algorithm to provably obtain Karush-Kuhn-Tucker (KKT) points of this problem.

## Index Terms

FDD massive MIMO, hybrid precoding, randomized control policy, channel sparsification.

**This work has been submitted to the IEEE for possible publication. Copyright may be transferred without notice, after which this version may no longer be accessible.**

\* State Key Laboratory of Advanced Optical Communication Systems and Networks, Department of Electronics, Peking University ( {tianch, luow}@pku.edu.cn ).

<sup>†</sup>College of Information Science and Electronic Engineering, Zhejiang University ( {anliu, mjzhao}@zju.edu.cn ) *Corresponding author: An Liu.*

<sup>‡</sup>Department of Telecommunication Systems, Technical University of Berlin ( {m.barzegarkhalilsarai, caire}@tu-berlin.de ).

## I. INTRODUCTION

Massive multiple-input multiple-output (MIMO) is considered as a promising technology for the development of future wireless networks, which will be spectrum-efficient, energy-efficient, secure, and robust [1]. With a large number of antennas employed at the base station (BS), more degrees of freedom (DoF) in the spatial domain are exploited to increase the capacity and simultaneously improve the energy efficiency by orders of magnitude [1], [2]. A well-known fact is that frequency division duplex (FDD) protocol dominates current wireless cellular systems [3], [4]. Also motivated by spectrum regulation issues, there is a significant commercial interest in enabling FDD massive MIMO to be compatible with current wireless networks [4]. However, two major challenges exist in FDD massive MIMO systems, as elaborated below.

**How to reduce the signaling overhead to obtain the channel state information at the transmitter (CSIT)?** The BS needs high-quality channel state information (CSI) to reap potential benefits of massive MIMO systems [1], [5]. In FDD massive MIMO systems, the acquisition of instantaneous CSI at the BS has to employ a closed-loop scheme because the channel reciprocity cannot be exploited anymore. The number of downlink training pilot symbols and CSI feedback signaling according to conventional channel estimation schemes, e.g., least squares (LS)-based methods, grows proportionally with the number of BS antennas, which leads to prohibitively large signaling overhead in FDD massive MIMO systems [6], [7]. To reduce the large portion of radio resources consumed by the overwhelming signaling overhead in FDD massive MIMO systems, compressive sensing (CS)-based approaches recently have been proposed [4], [8], [9], [10], based on the idea that high-dimensional wireless channels tend to exhibit sparse structures in the angular domain [7]. However, the significant signaling overhead reduction in all these works, relies heavily on the assumption of intrinsic sparse properties of propagation channels, which may not be satisfied in practice, especially for systems operating at sub-6G frequency.

**How to reduce the hardware cost and power consumption at the BS?** The traditional fully-digital precoder requires one radio frequency (RF) chain for each antenna at the BS, which leads to huge hardware cost and power consumption in massive MIMO systems [11]. To address this issue, hybrid precoding, which consists of a baseband digital precoder and a RF analog precoder, has been proposed [12], [13], [14]. However, the early works in [15], [16] require instantaneous CSI at the BS, which induces large CSI signaling overhead. Moreover, different RF precoders need to be implemented for different subcarriers since different subcarriers may

have different real-time CSI realizations [17]. To overcome this issue, [18], [19], [20] propose two-timescale hybrid precoding (THP) schemes, where the RF precoder is adaptive to channel statistics information to achieve array gain and the baseband precoder is adaptive to reduced dimensional effective CSI (product of channel and RF analog precoder) to achieve spatial multiplexing gain. Thus, the CSI signaling overhead can be significantly reduced. Furthermore, since the channel statistics are approximately same on different subcarriers [17], [21], THP only needs one RF precoder to cover all subbands, which makes it more charming in practice due to the significantly low implementation cost [17].

In existing works on (two-timescale) hybrid precoding, the analog precoder is designed to optimize the downlink transmission performance by assuming perfect knowledge of effective CSI. However, in practice, the analog precoder can influence the downlink transmission performance not only in directly affecting the spatial DoF of effective CSI, but also in directly affecting the quality of effective CSI estimation. The effect of analog precoding on the quality of effective CSI estimation is usually ignored in existing works. To achieve a better downlink transmission performance in practice, the optimization of analog precoding should also take into account the impact of analog precoding on the effective CSI estimation error. This question has been partially addressed in [22]. Specifically, to guarantee the estimation stability, i.e., the estimation error vanishes as the noise power tends to zero, [22] designs a sparsifying precoder to select active angular directions of each selected user, such that effective channels of all selected users are low-dimensional so that the stable estimation of effective channels can be achieved by the assigned limited number of pilot symbols. This active beam (angular direction)-user selection procedure is referred to as *active channel sparsification* in [22], which can be explained as the control of analog precoding on the impact of effective channel estimation error. Subject to the active channel sparsification constraint, the spatial DoF of effective CSI is maximized to achieve a good spectral efficiency.

However, there are some drawbacks in [22]: 1) The hybrid precoding scheme is not considered to reduce the hardware cost and power consumption. 2) It only considers sum-throughput maximization without the consideration of fairness among users. When the number of users is larger than the available spatial DoF, only a subset of users will be scheduled for transmission over a larger number of channel coherence intervals. 3) The channel sparsifying precoder is not designed to directly optimize the throughput performance, but is designed based on a heuristic

criteria.

In this paper, we propose a randomized channel sparsifying hybrid precoding (RCSHP) scheme to strike a balance between the spatial DoF of effective CSI and the effective CSI estimation error, so that the overall downlink transmission performance can be optimized with limited RF chains at the BS. The main contributions are summarized below.

- **Randomized analog precoding and power allocation:** In the proposed RCSHP, we consider a more flexible randomized analog precoding and power allocation scheme, which allows time-sharing between multiple analog precoders/power allocations, such that each analog precoder and power allocation can be used to cover a compatible user group. Moreover, both the time-sharing factors and the associated sets of analog precoders and power allocations are adapted to the channel covariance. Note that there is no need to explicitly do user grouping as it is automatically realized by optimizing the power allocation. Thus, this scheme resolves the fairness issue when the number of users is larger than the available spatial DoF. A motivating example of the randomized analog precoding and power allocation scheme at different time slots is shown in Fig. 1. At time slot 1 (Fig. 1a), the analog precoder and power allocation used at the BS are compatible with a group of users (user 1,2,5 and user 6), which can be simultaneously scheduled for transmission, but the other “incompatible” users (user 3 and user 4) can not be scheduled, i.e., the corresponding power allocation is zero due to the strong inter-user interference. However, at time slot 2 (Fig. 1b), the analog precoder and power allocation used at the BS is compatible with user 1, 2, 3 and user 4. Therefore, by time-sharing between these two analog precoders and power allocations, all users can enjoy a non-zero average data rate, achieving a better tradeoff between throughput performance and fairness. Note that in a compatible user group, the analog precoder should be chosen such that the effective CSI not only have enough spatial DoF to support simultaneous transmission to these users, but also are sparse enough to achieve a good effective CSI estimation quality under the limited downlink pilots. This indicates the proposed RCSHP can automatically achieve the active channel sparsification in [22] by optimizing the analog precoders, and thus is more robust w.r.t. various types of propagation environments.
- **Duality-based Digital precoder:** For a given analog precoder and power allocation, the digital precoder is adaptive to the estimated effective CSI to support multiuser-MIMO among

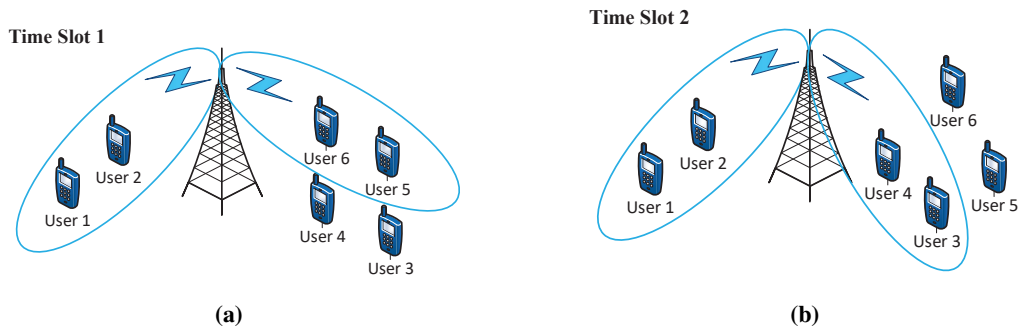


**Fig. 1:** An illustration of the randomized analog precoding and power allocation scheme at two time slots. (a) An example at time slot 1. (b) An example at time slot 2.

the users with non-zero transmit powers. In most existing works on hybrid precoding, the digital precoder is chosen to be regularized zero forcing (RZF) precoder [23] due to its low complexity and relatively good performance. However, RZF precoder is not a smooth function of the power allocation vector (as will be explained in Section II-D), making the direct optimization of power allocation intractable. In this paper, we propose a duality-based digital precoder to overcome this problem. By exploiting the fact that the precoding concepts designed for downlink transmission can be transformed to a virtual uplink reception [24], we equivalently obtain the duality-based digital precoder from a dual virtual uplink reception problem based on the minimum mean square error (MMSE) rule. The proposed duality-based digital precoder has similar complexity as RZF but can achieve better performance. Furthermore, it is a smooth function of the power allocation vector, leading to a tractable power allocation optimization formulation.

- **General utility optimization:** The time-sharing factors and associated sets of analog precoders and power allocations are jointly optimized to maximize a general utility function of long-term average data rates of users, including average weighted sum-rate maximization and proportional fairness (PFS) utility maximization as special cases. This problem is a challenging non-convex stochastic optimization problem. To address this problem, we propose an efficient stochastic successive convex approximation (SSCA) algorithm called SSCA-RCSHP. In addition, we also establish the convergence of SSCA-RCSHP algorithm to KKT solutions.

The rest of the paper is organized as follows. In Section II, we present the system model for FDD massive MIMO systems with hybrid precoding, the concept of randomized analog precoding and power allocation and the derivation of duality-based precoder. In Section III, we formulate the randomized channel sparsifying hybrid precoding design as a general utility problem. The proposed SSCA-RCSHP algorithm and associated convergence proof are presented in Section IV and V, respectively. Further, simulation results and conclusion are given in Section VI and VII, respectively.

*Notations:* The uppercase bold letter and lowercase bold letter denote the matrix and vector, respectively.  $\text{Diag}(\mathbf{a})$  represents a diagonal matrix whose diagonal elements form the vector  $\mathbf{a}$ .  $[\mathbf{M}]_{i\cdot}$ ,  $[\mathbf{M}]_{\cdot i}$  and  $[\mathbf{M}]_{ij}$  denote the  $i$ -th row,  $i$ -th column and  $(i, j)$ -th element of matrix  $\mathbf{M}$ , respectively.  $\otimes$  denotes Kronecker product and  $\circ$  denotes Hadamard product.  $\text{Tr}(\cdot)$ ,  $(\cdot)^*$ ,  $(\cdot)^T$ ,  $(\cdot)^H$ ,  $\|\cdot\|_1$ ,  $\|\cdot\|_F$ ,  $\mathbf{1}$  and  $\mathbf{I}$  denote trace, conjugate, transpose, conjugate transpose,  $l_1$  norm, Frobenius norm, all-one vector with appropriate size and identity matrix with appropriate size, respectively. Let  $\text{Vec}\{\mathbf{M}\}$  denote the vectorization of matrix  $\mathbf{M}$  and  $\Re[\mathbf{M}]$  denote the real part of a complex matrix  $\mathbf{M}$ .

## II. SYSTEM MODEL

### A. FDD Massive MIMO Downlink with Hybrid Precoding

Consider a multi-user FDD massive MIMO downlink system with one BS serving  $K$  single-antenna users. For clarity, we focus on a narrowband system with flat block fading channel, where the channel coefficients are assumed to be constant over a block containing  $T$  symbols, but the proposed problem formulation and algorithm can be also easily extended to the wideband system<sup>1</sup>. The BS employs the hybrid precoding architecture, as illustrated in Fig. 2, which is equipped with  $M$  antennas and  $S$  transmit RF chains, where  $S \ll M$ . It is necessary to clarify that the proposed scheme considers fairness in terms of the long-term average throughput. Thus the number of served users  $K$  is allowed to be more than the number of RF chains  $S$ , as long as the number of active users at each time slot is less than  $S$ . Moreover, a two-timescale hybrid precoder is employed to transmit data streams with limited RF chains. The transmit vector for user  $k$  is given by  $\sqrt{p_k} \mathbf{F} \mathbf{g}_k s_k$ , where  $\mathbf{F} \in \mathbb{C}^{M \times S}$  is the analog precoder,  $\mathbf{g}_k \in \mathbb{C}^{S \times 1}$  with

<sup>1</sup> In this paper, the analog precoder is adapted to the channel statistics only, and thus the same analog precoder will be used on different subcarriers in a wideband system. However, the digital precoders on different subcarriers can be different.

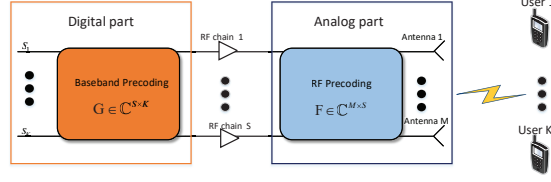


**Fig. 2:** Hybrid precoding architecture.

$\|\mathbf{F}\mathbf{g}_k\|_2 = 1$  is the  $k$ -th column vector of the normalized baseband digital precoder  $\mathbf{G} \in \mathbb{C}^{S \times K}$ ,  $p_k$  is the transmit power allocated to user  $k$  and  $s_k$  is the unity-power data symbol for user  $k$ . The analog precoder  $\mathbf{F}$  is adaptive to the channel statistics information to exploit array gain and sparsify the effective channel, and it is usually implemented using an RF phase shifting network<sup>2</sup> [25]. Hence, all elements of  $\mathbf{F}$  have equal magnitude and can be represented by a phase vector  $\boldsymbol{\theta} \in [0, 2\pi]^{MS}$ , i.e.,  $[\mathbf{F}]_{ij} = \frac{1}{\sqrt{M}}e^{\sqrt{-1}\theta_{ij}}$ , where  $\theta_{ij}$  is the phase of the  $(i, j)$ -th element of  $\mathbf{F}$  and corresponds to the  $((j-1)M + i)$ -th element of  $\boldsymbol{\theta}$ . The digital precoder  $\mathbf{G}$  is adaptive to the estimated effective CSI to achieve spatial multiplexing gain and mitigate inter-user interference. Under this setting, the received signal for user  $k$  is

$$y_k = \sqrt{p_k}\mathbf{h}_k^H\mathbf{F}\mathbf{g}_k s_k + \mathbf{h}_k^H \sum_{i \neq k} \sqrt{p_i}\mathbf{F}\mathbf{g}_i s_i + z_k, \quad (1)$$

where  $\mathbf{h}_k \in \mathbb{C}^M$  is the channel for user  $k$  and  $z_k \sim \mathcal{CN}(0, 1)$  is the normalized additive white Gaussian noise (AWGN).

### B. Randomized Analog Precoding and Power Allocation Policy

There may not always be enough spatial DoF to support simultaneous transmission to all users. For a fixed analog precoder, it is possible that only a subset of users can be scheduled for transmission over a larger number of time slots, when the number of users is larger than the available spatial DoF. Hence, for fairness consideration, we consider a randomized analog precoding and power allocation policy, which realizes time-sharing between several analog precoders/power allocations as defined below. The analog precoder and power allocation are together called composite control variable for the sake of conciseness.

<sup>2</sup> In practice, modern implementations are possible to allow for the full analog vector modulation, which means the analog precoder can be adjusted on both amplitude and phase. The proposed scheme can be easily modified to cover the analog precoder design using full vector modulators, actually just need to add the amplitude as an extra optimization variable.

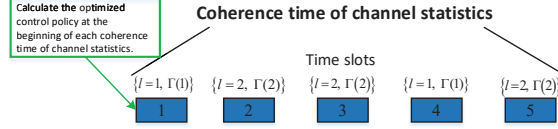


**Fig. 3:** A toy example of RCSHP.

**Definition 1.** (*Randomized Control Policy*): A randomized control policy  $\Omega = \{\Gamma, \mathbf{q}\}$  consists of an aggregated vector of  $L$  composite control variables  $\Gamma \triangleq [\Gamma(1)^T, \dots, \Gamma(L)^T]^T$  and a probability vector (time-sharing factors)  $\mathbf{q} \triangleq [q_1, \dots, q_L]^T$ , where the  $l$ -th composite control variable in  $\Gamma$  is  $\Gamma(l) = [\boldsymbol{\theta}(l)^T, \mathbf{p}(l)^T]^T$  and  $\Gamma$  satisfies  $\mathcal{G} = \{\boldsymbol{\theta}(l) \in [0, 2\pi]^{MS}, \mathbf{p}(l) \in \mathbb{R}_+^K, \forall l\}$ , and  $\mathbf{q}$  satisfies  $\mathcal{Q} = \{\mathbf{q} \in [0, 1]^L, \mathbf{1}^T \mathbf{q} = 1\}$ . At any time slot, the composite control variable  $\Gamma(l)$  is used with probability  $q_l$ , i.e., the analog precoder and power allocation are respectively given by  $\boldsymbol{\theta}(l)$  and  $\mathbf{p}(l)$  with probability  $q_l$ .

In the proposed RCSHP, the composite control variables and associated time-sharing factors are first jointly optimized according to the channel statistics information at the beginning of each coherence time of channel statistics. Coherence time of channel statistics refers to the time interval when the channel statistics remain unchanged. Then the optimized control policy is applied to time slots of the current coherence time of channel statistics to realize time-sharing between different composite control variables. Clearly, choosing a larger  $L$  always leads to a better performance since a control policy with a larger  $L$  includes that with a smaller  $L$  as a special case. However, the complexity of the optimization algorithm will also increase with  $L$ . As such, we can use  $L$  to control the tradeoff between the performance and complexity. In the simulations, we find that a moderately large  $L$  (4 or 5) can already achieve a good performance.

We use a toy example shown in Fig. 3 to illustrate the proposed RCSHP. The RCSHP in this example is specified by a set of  $L = 2$  composite control variables  $\Gamma = [\Gamma(1)^T, \Gamma(2)^T]^T$  and a time-sharing factor  $\mathbf{q} = [0.4, 0.6]^T$ , where  $\Gamma(1)$  and  $\Gamma(2)$  are the analog precoder and power allocation corresponding to Fig. 1a and Fig. 1b, respectively. For convenience, we assume the current coherence time of channel statistics consists of 5 time slots. One possible realization of RCSHP is illustrated in Fig. 3. In this example,  $\Gamma(1)$  and  $\Gamma(2)$  are used in 40% and 60% of time slots, respectively.

### C. Instantaneous Effective CSI Estimation

The effective CSI estimation quality has a significant impact on the downlink transmission performance. We consider a closed-loop scheme to estimate the instantaneous effective CSI, where the BS sends a sequence of  $T_p$  pilot symbols through the  $S$  inputs of analog precoder  $\mathbf{F}$  to all users and each user feeds back its pilot observation. The estimation of effective CSI for each user is then implemented at the BS. Denote the aggregate common transmitted pilot symbols as  $\mathbf{\Psi} \in \mathbb{C}^{T_p \times S}$ . The corresponding pilot observation at user  $k$  is

$$\mathbf{y}_k^{\text{pilot}} = \mathbf{\Psi} (\mathbf{h}_k^H \mathbf{F})^H + \mathbf{n}_k = \mathbf{\Psi} \tilde{\mathbf{h}}_k + \mathbf{n}_k, \quad (2)$$

where  $\tilde{\mathbf{h}}_k = \mathbf{F}^H \mathbf{h}_k$  is the effective channel of user  $k$  and the aggregated effective channel matrix is given by  $\tilde{\mathbf{H}} = \mathbf{H} \mathbf{F} = [\tilde{\mathbf{h}}_1, \dots, \tilde{\mathbf{h}}_K]^H$ , and the channel estimation noise is normalized AWGN with distribution  $\mathbf{n}_k \sim \mathcal{CN}(\mathbf{0}, \mathbf{I})$ .

Similar to [22], we assume noiseless analog feedback for clarity consideration, but the proposed scheme can be easily modified to consider noisy feedback. The BS implements linear minimum mean square error (LMMSE) estimation to estimate the effective CSI, since the estimation quality using LMMSE is already good enough when the dimension of effective CSI is less than the number of pilot symbols. Thus the LMMSE estimation of the effective channel for user  $k$  is

$$\hat{\tilde{\mathbf{h}}}_k = \mathbf{F}^H \mathbf{C}_k \mathbf{F} \mathbf{\Psi}^H (\mathbf{\Psi} \mathbf{F}^H \mathbf{C}_k \mathbf{F} \mathbf{\Psi}^H + \mathbf{I})^{-1} \mathbf{y}_k^{\text{pilot}}, \quad (3)$$

where  $\mathbf{C}_k \in \mathbb{C}^{M \times M}$  is the channel covariance of user  $k$ .

In our scheme, the channel covariances  $\mathbf{C}_k, \forall k$  are assumed to be known at the BS. It is reasonable since there are many efficient channel covariance estimation methods in the hybrid precoding architecture. Please refer to [26], [27] and references therein. Moreover, by exploiting the downlink/uplink angle reciprocity, the downlink channel covariance can be obtained from uplink training pilots even in FDD systems. Please refer to [22], [28] and references therein.

### D. Duality-based Digital Precoder

We propose a duality-based digital precoder by exploiting the duality between the multi-user downlink system and the corresponding virtual uplink system [24]. Specifically, for a given analog precoder  $\mathbf{F}$  and downlink power allocation  $\mathbf{p}_{\text{dl}} = [p_{\text{dl},1}, \dots, p_{\text{dl},K}]^T$  which satisfies the sum-power constraint  $\|\mathbf{p}_{\text{dl}}\|_1 \leq P_{\text{max}}$ , the downlink system model is illustrated in Fig. 4a, where  $\mathbf{P}_{\text{dl}}$  denotes

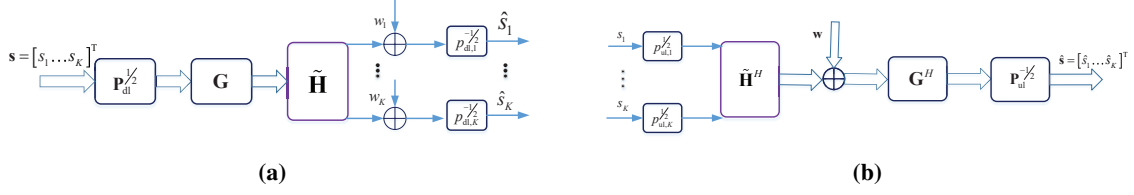


**Fig. 4:** An illustration of the downlink system model and equivalent virtual uplink system model. (a) Downlink system model. (b) Equivalent virtual uplink system model.

$\text{Diag}(\mathbf{p}_{\text{dl}})$ . The corresponding virtual uplink model is obtained by switching the role of transmitter and receiver. The data symbol vector  $\mathbf{s}$  is transmitted from  $K$  independent users through the channel  $\tilde{\mathbf{H}}^{\text{H}}$ .  $\mathbf{G}^{\text{H}}$  now behaves as a normalized multi-user receiver. The quantities  $\mathbf{G}, \tilde{\mathbf{H}}$  remains the same as the downlink system. The uplink power allocation  $\mathbf{p}_{\text{ul}} = [p_{\text{ul},1}, \dots, p_{\text{ul},K}]^{\text{T}}$  satisfies the same sum-power constraint as the downlink, i.e.,  $\|\mathbf{p}_{\text{ul}}\|_1 \leq P_{\text{max}}$ . The duality theory established in [29], [24] shows that the downlink and virtual uplink can achieve the same data rate region. Moreover, the Pareto-optimal precoder that achieves a boundary point of the data rate region in the downlink is given by the MMSE receiver in the virtual uplink corresponding to the same Pareto-optimal rate point. Motivated by this duality theory, we obtain the digital precoder (called duality-based precoder) from the virtual uplink MMSE receiver.

In particular, for a given power allocation  $\mathbf{p}$ , the MMSE receiver in the virtual uplink is given by

$$\mathbf{G}^{\text{mmse}} = \left( \tilde{\mathbf{H}}^{\text{H}} \mathbf{P} \tilde{\mathbf{H}} + \mathbf{I} \right)^{-1} \tilde{\mathbf{H}}^{\text{H}} \mathbf{P}. \quad (4)$$

where  $\mathbf{P} = \text{Diag}(\mathbf{p})$ . Then the baseband digital precoder  $\mathbf{G}$  in the downlink is given by

$$\mathbf{G} = \left( \tilde{\mathbf{H}}^{\text{H}} \mathbf{P} \tilde{\mathbf{H}} + \mathbf{I} \right)^{-1} \tilde{\mathbf{H}}^{\text{H}} \mathbf{P} \boldsymbol{\Lambda}^{\frac{1}{2}}, \quad (5)$$

where  $\boldsymbol{\Lambda}^{\frac{1}{2}} = \text{Diag}([\|\tilde{\mathbf{g}}_1\|^{-1}, \dots, \|\tilde{\mathbf{g}}_K\|^{-1}])$  is used to normalize the precoding vectors  $\mathbf{F}\mathbf{g}_k$ 's, and  $\tilde{\mathbf{g}}_k$  is the  $k$ -th column of  $\tilde{\mathbf{G}} \triangleq \mathbf{F} \left( \tilde{\mathbf{H}}^{\text{H}} \mathbf{P} \tilde{\mathbf{H}} + \mathbf{I} \right)^{-1} \tilde{\mathbf{H}}^{\text{H}} \mathbf{P}$ .

As a comparison, the RZF digital precoder [23] is given by

$$\mathbf{G}_{\text{RZF}} = \tilde{\mathbf{H}}^{\text{H}} \left( \tilde{\mathbf{H}} \tilde{\mathbf{H}}^{\text{H}} + \alpha \mathbf{I} \right)^{-1} \boldsymbol{\Upsilon}^{\frac{1}{2}}, \quad (6)$$

where  $\boldsymbol{\Upsilon}^{\frac{1}{2}} = \text{Diag}([\|\tilde{\mathbf{g}}_1\|^{-1}, \dots, \|\tilde{\mathbf{g}}_K\|^{-1}])$  is used to normalize the column vectors of  $\mathbf{F}\mathbf{G}_{\text{RZF}}$ ,  $\tilde{\mathbf{g}}_k$  is the  $k$ -th column of  $\tilde{\mathbf{G}} \triangleq \mathbf{F} \tilde{\mathbf{H}}^{\text{H}} \left( \tilde{\mathbf{H}} \tilde{\mathbf{H}}^{\text{H}} + \alpha \mathbf{I} \right)^{-1}$  and  $\alpha$  is the regularization factor. In (6), the RZF precoder is obtained by assuming that all  $K$  users are scheduled for transmission. A

well-known fact is that the RZF precoder requires explicit user-selection to achieve a good spatial multiplexing gain. The set of scheduled users can essentially be expressed as an indicator function<sup>3</sup> of power allocation. Thus, the RZF precoder is not a smooth function of power allocation, making the direct optimization of power allocation intractable. In contrast, the duality-based precoder  $\mathbf{G}$  in (5) is obviously a smooth function of power allocation, leading to a tractable power allocation optimization<sup>4</sup>, which can meanwhile do implicit user-selection by optimizing the power allocation. Moreover, the complexity of duality-based precoder  $\mathbf{G}$  in (5) is similar with the RZF precoder  $\mathbf{G}_{\text{RZF}}$ .

Another interesting observation is that the RZF precoder is a special case of the duality-based precoder for a certain choice of power allocation. For example, apply an equal power allocation, i.e.,  $p_k = p = \frac{P_{\max}}{K}, \forall k$ , to duality-based precoder  $\mathbf{G}$  in (5). Then from the matrix inverse lemma, it can be verified that  $\mathbf{G}$  (unnormalized form) degrades to the RZF precoder  $\mathbf{G}_{\text{RZF}}$  (unnormalized form) with  $\alpha = \frac{1}{p}$  as

$$\mathbf{G} = \mathbf{G}_{\text{RZF}} = \tilde{\mathbf{H}}^{\text{H}} \left( \tilde{\mathbf{H}}\tilde{\mathbf{H}}^{\text{H}} + \frac{1}{p}\mathbf{I} \right)^{-1}.$$

Since  $\alpha = \frac{1}{p}$  is the asymptotic optimal regularization factor for the RZF precoder under perfect CSI [23], [30], this further indicates the performance of duality-based precoder after power allocation optimization will be better than the RZF precoder.

Considering the impact of effective CSI estimation error, the final baseband digital precoder  $\mathbf{G}$  is given by

$$\mathbf{G} = \left( \begin{matrix} \hat{\mathbf{H}}^{\text{H}} & \hat{\mathbf{H}} \\ \hat{\mathbf{H}} & \mathbf{P}\hat{\mathbf{H}} \end{matrix} + \mathbf{I} \right)^{-1} \begin{matrix} \hat{\mathbf{H}}^{\text{H}} \\ \hat{\mathbf{H}} \end{matrix} \mathbf{P}\mathbf{\Lambda}^{\frac{1}{2}}. \quad (7)$$

where  $\hat{\mathbf{H}} = \left[ \hat{\mathbf{h}}_1, \dots, \hat{\mathbf{h}}_K \right]^{\text{H}}$  is the estimated effective CSI matrix and  $\mathbf{\Lambda}^{\frac{1}{2}}$  is the corresponding normalization matrix.

### E. Achievable Data Rate

In the proposed RCSHP, we consider the randomized control policy as elaborated in section II-B. Under a given realization of control state  $l$ , the composite control variable is given by

<sup>3</sup> Specifically, the power allocated to user  $k$  under the RZF precoder is given by  $p_k \mathbb{1}(k \in \mathcal{U})$ , where  $\mathcal{U}$  is the scheduled user set after explicit user selection.

<sup>4</sup> The tractable power allocation optimization in this paper means that we can develop an efficient low complexity algorithm to find a “good” KKT point without having to deal with the more complicated combinatorial optimization of user selection. The power allocation optimization problem may still be non-convex.

$\Gamma(l) = [\boldsymbol{\theta}(l)^\top, \mathbf{p}(l)^\top]^\top$ , where  $\boldsymbol{\theta}(l)$  and  $\mathbf{p}(l)$  are the phase shifting vector of RF precoder  $\mathbf{F}(l)$  and power allocation vector in control state  $l$ , respectively. For a given channel realization  $\mathbf{H}$  and channel estimation noise realization  $\mathbf{N} = [\mathbf{n}_1, \dots, \mathbf{n}_K]^\text{H}$ , the instantaneous achievable data rate of user  $k$  in control state  $l$  is

$$r_k(\Gamma(l); \mathbf{H}, \mathbf{N}, l) = \log \left( 1 + \frac{p_k |\mathbf{h}_k^\text{H} \mathbf{F} \mathbf{g}_k|^2}{\sum_{i \neq k} p_i |\mathbf{h}_k^\text{H} \mathbf{F} \mathbf{g}_i|^2 + 1} \right), \quad (8)$$

where the control state  $l$  is dropped off in the specific expression of  $r_k$  for conciseness consideration. Note that  $\mathbf{F}$  is a function of  $\boldsymbol{\theta}(l)$  and  $\mathbf{G}$  is a function of  $\boldsymbol{\theta}(l), \mathbf{p}(l), \mathbf{H}, \mathbf{N}$ . Thus we explicitly express  $r_k$  as a function of  $\Gamma(l)$  which depends on the random states  $\mathbf{H}, \mathbf{N}, l$ . Then for a given control policy  $\Omega = \{\Gamma, \mathbf{q}\}$ , the average achievable data rate of user  $k$  is given by

$$\bar{r}_k = \sum_{l=1}^L q_l \mathbb{E}_{\mathbf{H}, \mathbf{N}} [r_k(\Gamma(l); \mathbf{H}, \mathbf{N}, l)]. \quad (9)$$

Define  $\bar{\mathbf{r}} \triangleq [\bar{r}_1, \dots, \bar{r}_K]^\top$  as the average data rate vector.

### III. PROBLEM FORMULATION

The joint optimization of the randomized control policy, i.e., the time-sharing factors and the associated sets of analog precoders and power allocations, can be formulated as the following general utility maximization problem:

$$\mathcal{P} : \quad \max_{\Gamma \in \mathcal{G}, \mathbf{q} \in \mathcal{Q}} \quad f(\Gamma, \mathbf{q}) \triangleq U(\bar{\mathbf{r}}) \quad (10a)$$

$$\text{s.t.} \quad \mathbf{1}^\top \mathbf{p}(l) \leq P_{\max} \quad l = 1, \dots, L, \quad (10b)$$

where  $P_{\max}$  is the transmit power budget at the BS.  $U(\cdot)$  is a general utility function, which is assumed to be continuously differentiable, concave and nondecreasing for all  $\bar{\mathbf{r}} \geq 0$ , and the gradient of  $U(\bar{\mathbf{r}})$  w.r.t.  $\bar{\mathbf{r}}$  is Lipschitz continuous. This general utility function  $U(\bar{\mathbf{r}})$  includes many important network utilities as special cases, such as alpha-fair utility [31], sum rate ( $U(\bar{\mathbf{r}}) = \sum_{k=1}^K \bar{r}_k$ , a special case of alpha-fair when  $\alpha = 0$ ) and proportional fairness utility ( $U(\bar{\mathbf{r}}) = \sum_{k=1}^K \log(\bar{r}_k + \epsilon)$ , where  $\epsilon > 0$  is a small number to avoid the singularity at  $\bar{r}_k = 0$ , also a special case of alpha-fair when  $\alpha = 1$ ).

Assume a Gaussian channel model, i.e.,  $\mathbf{h}_k \sim \mathcal{CN}(\mathbf{0}, \mathbf{C}_k), \forall k$ , for the convenient design consideration as similar to [22]. In our design, the randomized control policy is assumed to be adaptive to the channel covariance (channel statistics information). This assumption is reasonable

because the “channel hardening” [32] in massive MIMO system leads to that the gain of adapting the randomized control policy according to the instantaneous CSI is small [11], [30]. Then at the beginning of each coherence time of channel statistics, we can firstly generate appropriate number of channel samples and channel estimation noise samples according to the statistical CSI  $\mathcal{H}$ , i.e., the channel distribution  $\mathbf{h}_k \sim \mathcal{CN}(\mathbf{0}, \mathbf{C}_k)$ ,  $\forall k$ , and channel estimation noise distribution  $\mathbf{n}_k \sim \mathcal{CN}(\mathbf{0}, \mathbf{I})$ ,  $\forall k$ , to solve problem  $\mathcal{P}$  in order to obtain the optimized randomized control policy  $\Omega^* = \{\Gamma^*, \mathbf{q}^*\}$ .

During the maximization of utility, the dimension of effective channel tends to be smaller than the number of pilot symbols  $T_p$  so that the channel sparsifying is implicitly realized by optimizing the analog precoders, leading to an improved effective CSI estimation quality. Meanwhile, the user-selection/grouping procedure is also implicitly realized by optimizing power allocations. Thus, the active channel sparsification and excellent downlink transmission can be achieved simultaneously by maximizing the utility function over the randomized control policy. Each optimized composite control variable corresponds to a compatible group of users, such that the effective CSI not only has enough spatial DoF to support simultaneous transmission to these users, but also is sparse enough to achieve a good effective CSI estimation quality by the limited downlink pilots. After the optimized randomized control policy  $\Omega^*$  has been calculated, we simply apply it at each time slot during the current coherence time of channel statistics and the baseband precoder  $\mathbf{G}$  is adaptive to the instantaneous effective CSI to support downlink transmission. A toy example has been elaborated in section II-B and the illustration is shown in Fig. 3.

However, there are several challenges in finding KKT solutions of problem  $\mathcal{P}$ , as elaborated below. First, the objective function is neither convex nor concave and it contains expectation operators, which usually do not have closed-form expressions. Moreover, there are three random system states  $\mathbf{H}, \mathbf{N}$  and  $l$ , and the probability measure of the control state  $l$  depends on the time-sharing vector  $\mathbf{q}$ . We propose an efficient SSCA-RCSHP algorithm to find KKT points of problem  $\mathcal{P}$ .

#### IV. ALGORITHM DESIGN

In this section, we propose an efficient stochastic SCA algorithm called SSCA-RCSHP to solve problem  $\mathcal{P}$ . Algorithm 1 summarizes the key steps of the SSCA-RCSHP. At each iteration

$t$ , the randomized control policy  $\Omega = \{\Gamma, \mathbf{q}\}$  is updated by solving a convex surrogate problem obtained by replacing the objective function  $f(\Gamma, \mathbf{q})$  with its surrogate function  $\bar{f}^t(\Gamma, \mathbf{q})$ .

Specifically, at  $t$ -th iteration,  $T_{HN}$  new channel realizations and new channel estimation noise realizations  $\{\mathbf{H}^t(i), \mathbf{N}^t(i)\}_{i=1, \dots, T_{HN}}$  are firstly generated according to the statistical CSI  $\mathcal{H}$  in Step 1. Then the surrogate function  $\bar{f}^t(\mathbf{q}, \Gamma)$  is updated based on  $\{\mathbf{H}^t(i), \mathbf{N}^t(i)\}_{i=1, \dots, T_{HN}}$  and the current iterate  $\mathbf{q}^t, \Gamma^t$  in Step 2 as

$$\begin{aligned} \bar{f}^t(\Gamma, \mathbf{q}) = & U(\hat{\mathbf{r}}^t(\mathbf{q})) - \tau_q \|\mathbf{q} - \mathbf{q}^t\|^2 \\ & + (\mathbf{f}_\Gamma^t)^\top (\Gamma - \Gamma^t) - \tau_\Gamma \|\Gamma - \Gamma^t\|^2, \end{aligned} \quad (11)$$

where  $\tau_q, \tau_\Gamma > 0$  are two constants,  $\hat{\mathbf{r}}^t(\mathbf{q}) = \left[ \sum_{l=1}^L q_l \hat{r}_1^t(l), \dots, \sum_{l=1}^L q_l \hat{r}_K^t(l) \right]^\top$  is an approximation for the average data rate vector and  $\hat{r}_k^t(l)$  is the approximate conditional average data rate of user  $k$  under  $l$ -th analog precoding and power allocation state, which is recursively updated as

$$\begin{aligned} \hat{r}_k^t(l) = & (1 - \rho_t) \hat{r}_k^{t-1}(l) + \\ & \rho_t \sum_{i=1}^{T_{HN}} \frac{r_k(\Gamma^t(l); \mathbf{H}^t(i), \mathbf{N}^t(i))}{T_{HN}}, \forall k, \forall l, \end{aligned} \quad (12)$$

with  $\hat{r}_k^{-1} = 0, \forall k, \forall l$ .  $\mathbf{f}_\Gamma^t$  is an approximation of the partial derivative  $\nabla_\Gamma U(\bar{\mathbf{r}})$ , which is updated recursively as

$$\begin{aligned} \mathbf{f}_\Gamma^t = & (1 - \rho_t) \mathbf{f}_\Gamma^{t-1} \\ & + \rho_t \sum_{i=1}^{T_{HN}} \frac{\mathbf{J}_\Gamma(\Gamma^t, \mathbf{q}^t; \mathbf{H}^t(i), \mathbf{N}^t(i)) \nabla_{\bar{\mathbf{r}}} U(\hat{\mathbf{r}}^t(\mathbf{q}^t))}{T_{HN}}, \end{aligned} \quad (13)$$

with  $\mathbf{f}_\Gamma^{-1} = \mathbf{0}$ , where  $\mathbf{f}_\Gamma^t = \left[ \left( \mathbf{f}_{\Gamma(1)}^t \right)^\top, \dots, \left( \mathbf{f}_{\Gamma(l)}^t \right)^\top, \dots, \left( \mathbf{f}_{\Gamma(L)}^t \right)^\top \right]^\top$ ,  $\rho_t \in (0, 1]$  is a sequence to be properly chosen,  $\mathbf{J}_\Gamma(\Gamma, \mathbf{q}; \mathbf{H}, \mathbf{N})$  is the Jacobian matrix of the data rate vector  $\tilde{\mathbf{r}}(\Gamma, \mathbf{q}; \mathbf{H}, \mathbf{N}) = \left[ \sum_{l=1}^L q_l r_1(l), \dots, \sum_{l=1}^L q_l r_K(l) \right]^\top$  w.r.t.  $\Gamma$  and its detailed expression is given by Appendix A. Clearly, the sample size  $T_{HN}$  can be chosen to control the tradeoff between complexity and convergence speed.

After updating the surrogate function, the following surrogate function maximization problem is firstly solved:

$$\hat{\mathcal{P}} : \quad \max_{\Gamma \in \mathcal{G}, \mathbf{q} \in \mathcal{Q}} \quad \bar{f}^t(\Gamma, \mathbf{q}) \quad (14a)$$

$$\text{s.t.} \quad \mathbf{1}^\top \mathbf{p}(l) \leq P_{\max} \quad l = 1, \dots, L. \quad (14b)$$

Then the control policy is updated based on the solution of  $\widehat{\mathcal{P}}$ , as summarized in Step 3 and 4.

Specifically, the problem  $\widehat{\mathcal{P}}$  can be decomposed into  $L + 1$  convex subproblems w.r.t.  $\mathbf{q}$  and  $\mathbf{\Gamma}(l), \forall l$ , respectively. Thus in Step 3a, the optimal solution  $\bar{\mathbf{q}}^t$  for  $\widehat{\mathcal{P}}$  is obtained by solving the following subproblem:

$$\mathcal{P}_q : \quad \bar{\mathbf{q}}^t = \arg \max_{\mathbf{q} \in \mathcal{Q}} U(\hat{\mathbf{r}}^t(\mathbf{q})) - \tau_q \|\mathbf{q} - \mathbf{q}^t\|^2, \quad (15)$$

where the proximal term  $\tau_q \|\mathbf{q} - \mathbf{q}^t\|^2$  guarantees problem  $\mathcal{P}_q$  strongly convex. This subproblem can be solved by standard convex optimization methods [33]. Then the time-sharing vector  $\mathbf{q}$  is updated in Step 3b as

$$\mathbf{q}^{t+1} = (1 - \gamma_t) \mathbf{q}^t + \gamma_t \bar{\mathbf{q}}^t. \quad (16)$$

In Step 4a, the optimal solution  $\bar{\mathbf{\Gamma}}^t = [(\bar{\mathbf{\Gamma}}^t(1))^T, \dots, (\bar{\mathbf{\Gamma}}^t(L))^T]^T$  for  $\widehat{\mathcal{P}}$  is obtained by independently solving the following  $L$  subproblems:

$$\begin{aligned} \mathcal{P}_{\Gamma_l} : \quad \bar{\mathbf{\Gamma}}^t(l) = \arg \max_{\mathbf{\Gamma}(l) \in \mathcal{G}_l} & (\mathbf{f}_{\mathbf{\Gamma}(l)}^t)^T (\mathbf{\Gamma}(l) - \mathbf{\Gamma}^t(l)) \\ & - \tau_{\Gamma} \|\mathbf{\Gamma}(l) - \mathbf{\Gamma}^t(l)\|^2, \end{aligned} \quad (17)$$

$$\text{s.t.} \quad \mathbf{1}^T \mathbf{p}(l) \leq P_{\max},$$

for  $l = 1, \dots, L$ , where  $\mathcal{G}_l = \{\boldsymbol{\theta}(l) \in [0, 2\pi]^{MS}, \mathbf{p}(l) \in \mathbb{R}_+^K\}$ .

Problem  $\mathcal{P}_{\Gamma_l}$  is a convex problem, which can be efficiently solved by the Lagrange dual method. In particular, denote  $\bar{\mathbf{1}} = [\mathbf{0}_{MS \times 1}^T, \mathbf{1}_{K \times 1}^T]^T$ , then the Lagrange function for (17) is

$$\mathcal{L}(\mathbf{\Gamma}(l), \lambda) = -\tau_{\Gamma} \|\mathbf{\Gamma}(l)\|_2^2 + \mathbf{b}_l^T(\lambda) \mathbf{\Gamma}(l) + c_l(\lambda), \mathbf{\Gamma}(l) \in \mathcal{G}_l,$$

where  $\lambda \in \mathbb{R}_+$  is the Lagrange multiplier (which is also called dual variable) and

$$\mathbf{b}_l(\lambda) = \mathbf{f}_{\mathbf{\Gamma}(l)}^t + 2\tau_{\Gamma} \mathbf{\Gamma}^t(l) - \lambda \bar{\mathbf{1}},$$

$$c_l(\lambda) = \lambda P_{\max} - (\mathbf{f}_{\mathbf{\Gamma}(l)}^t)^T \mathbf{\Gamma}^t(l) - \tau_{\Gamma} \|\mathbf{\Gamma}^t(l)\|_2^2.$$

The dual function for (17) is

$$g^l(\lambda) = \max_{\mathbf{\Gamma}(l) \in \mathcal{G}_l} \mathcal{L}(\mathbf{\Gamma}(l), \lambda). \quad (18)$$

And the corresponding dual problem is

$$\min_{\lambda \geq 0} g^l(\lambda). \quad (19)$$

---

**Algorithm 1** SSCA-RCSHP Algorithm

---

**Initialize:**  $\Gamma^0, \mathbf{q}^0, \hat{r}_k^{-1} = 0, \forall k, \mathbf{f}_\Gamma^{-1} = 0, T_{HN}, t = 0.$

**Step 1:** Generate  $T_{HN}$  new channel realizations and new channel estimation noise realizations  $\{\mathbf{H}^t(i), \mathbf{N}^t(i)\}_{i=1, \dots, T_{HN}}$  according to the statistical CSI  $\mathcal{H}$  at  $t$ -th iteration.

**Step 2:** Update the surrogate function by (11).

**Step 3a:** Solve (15) to obtain the optimal solution  $\bar{\mathbf{q}}^t.$

**Step 3b:** Update  $\mathbf{q}^{t+1}$  according to (16).

**Step 4a:** Distributedly solve  $L$  subproblems (17) to obtain the optimal solution  $\bar{\Gamma}^t.$

**Step 4b:** Update  $\Gamma^{t+1}$  according to (21).

**Step 5:** Let  $t = t + 1$  and return to Step 1.

---

For a fixed Lagrange multiplier  $\lambda$ , the optimal  $\Gamma^\circ(l, \lambda)$  for the maximization problem in (18) has a closed-form expression, which is given by

$$\Gamma^\circ(l, \lambda) = \mathbb{P}_{\mathcal{G}_l} \left[ \Gamma^t(l) + \frac{\mathbf{f}_{\Gamma^t(l)} - \lambda \bar{\mathbf{1}}}{2\tau_\Gamma} \right], \quad (20)$$

where  $\mathbb{P}_{\mathcal{G}_l}[\cdot]$  denotes the projection onto the convex set  $\mathcal{G}_l$ . Then use bisection search to find the optimal Lagrange multiplier  $\lambda^\circ$  for dual problem (19) and the optimal primal solution of  $\mathcal{P}_{\Gamma_l}$  is given by  $\bar{\Gamma}^t(l) = \Gamma^\circ(l, \lambda^\circ).$

Subsequently, the aggregate vector of control variables  $\Gamma$  is updated in Step 4b according to

$$\Gamma^{t+1} = (1 - \gamma_t) \Gamma^t + \gamma_t \bar{\Gamma}^t, \quad (21)$$

where  $\gamma_t \in (0, 1]$  is a sequence to be properly chosen. Then the above steps (Step 1 to Step 4) are carried out until convergence.

## V. CONVERGENCE ANALYSIS

In this section, we establish the convergence of SSCA-RCSHP to KKT solutions. Notice that the limiting point is obtained by averaging over all the previous solutions from the surrogate problem (14), which makes it difficult to show that the limiting point is a KKT point of the original Problem (10). To address this challenge, we need to make some assumptions on the sequence of parameters  $\{\rho_t\}$  and  $\{\gamma_t\}$ .

**Assumption 1.** (*Assumptions on  $\{\rho_t\}, \{\gamma_t\}$* ):

- 1)  $\rho_t \rightarrow 0$ ,  $\frac{1}{\rho_t} \leq O(t^\beta)$  for some  $\beta \in (0, 1)$ ,  $\sum_t (\rho_t)^2 < \infty$ ,  $\sum_t \rho_t t^{-\frac{1}{2}} < \infty$ .
- 2)  $\gamma_t \rightarrow 0$ ,  $\sum_t \gamma_t = \infty$ ,  $\sum_t (\gamma_t)^2 < \infty$
- 3)  $\lim_{t \rightarrow \infty} \frac{\gamma_t}{\rho_t} = 0$

Note that the condition  $\frac{1}{\rho_t} \leq O(t^\beta)$  for some  $\beta \in (0, 1)$  is almost the same as  $\sum_t \rho_t = \infty$ , which is a common assumption in stochastic optimization algorithms [34]. With Assumption 1, we first prove a key lemma that will support the final convergence. The following lemma proves the convergence of the surrogate objective function.

**Lemma 1.** (*Convergence of the surrogate objective function*): *Suppose Assumptions 1 are satisfied. Consider a subsequence  $\{\Gamma^{t_j}, \mathbf{q}^{t_j}\}_{j=1}^\infty$  converging to a limiting point  $\{\Gamma^*, \mathbf{q}^*\}$ , and define a function*

$$\begin{aligned} \hat{f}(\Gamma, \mathbf{q}) &\triangleq U(\bar{\mathbf{r}}(\Gamma^*, \mathbf{q})) - \tau_q \|\mathbf{q} - \mathbf{q}^*\|^2 \\ &\quad + \nabla_{\Gamma}^T f(\Gamma^*, \mathbf{q}^*) (\Gamma - \Gamma^*) - \tau_{\Gamma} \|\Gamma - \Gamma^*\|^2, \end{aligned}$$

which satisfies  $\hat{f}(\Gamma^*, \mathbf{q}^*) = f(\Gamma^*, \mathbf{q}^*)$ ,  $\nabla_{\Gamma} \hat{f}(\Gamma^*, \mathbf{q}^*) = \nabla_{\Gamma} f(\Gamma^*, \mathbf{q}^*)$  and  $\nabla_{\mathbf{q}} \hat{f}(\Gamma^*, \mathbf{q}^*) = \nabla_{\mathbf{q}} f(\Gamma^*, \mathbf{q}^*)$ . Then almost surely, we have

$$\lim_{j \rightarrow \infty} \bar{f}^{t_j}(\Gamma, \mathbf{q}) = \hat{f}(\Gamma, \mathbf{q}), \forall \mathbf{q} \in \mathcal{Q}, \forall \Gamma \in \mathcal{X},$$

where  $\mathcal{Q} = \{\mathbf{q} \in [0, 1]^L, \mathbf{1}^T \mathbf{q} = 1\}$  and  $\mathcal{X} = \{\boldsymbol{\theta}(l) \in [0, 2\pi]^{MS}, \mathbf{p}(l) \in \mathbb{R}_+^K, \mathbf{1}^T \mathbf{p}(l) \leq P_{\max}, \forall l\}$  are the feasible sets of  $\mathbf{q}$  and  $\Gamma$ , respectively.

Please refer to Appendix B for the proof. With Lemma 1, the following convergence theorem can be proved.

**Theorem 1.** (*Convergence of Algorithm 1*): *Suppose Assumptions 1 are satisfied. For any subsequence  $\{\Gamma^{t_j}, \mathbf{q}^{t_j}\}_{j=1}^\infty$  converging to a limiting point  $\{\Gamma^*, \mathbf{q}^*\}$ ,  $\{\Gamma^*, \mathbf{q}^*\}$  is a KKT point of Problem (10) almost surely.*

Please refer to Appendix C for the proof.

## VI. SIMULATION RESULTS

In this section, we compare the performance of RCSHP with the active channel sparsification (ACS) scheme in [22] and two-timescale hybrid precoding (THP) scheme in [11]. As in [11]

and [22], we adopt a geometry-based channel model and a COST 2100 channel model, both with a half-wavelength spaced uniform linear array (ULA) for simulations. For the geometry-based channel model, the channel vector of user  $k$  can be expressed as  $\mathbf{h}_k = \sum_{i=1}^{N_p} \alpha_{k,i} \mathbf{a}(\varphi_{k,i})$ , where  $\mathbf{a}(\varphi) = [1, e^{j\pi \sin(\varphi)}, \dots, e^{j(M-1)\pi \sin(\varphi)}]^T$  is the array response vector,  $\varphi_{k,i}$ 's are angles of departure (AoD) which are Laplacian distributed with an angle spread  $\sigma_{AS} = 10$  and  $\alpha_{k,i} \sim \mathcal{CN}(0, \sigma_{k,i}^2)$ ,  $\sigma_{k,i}^2$ 's are randomly generated from an exponential distribution and normalized such that  $\sum_{i=1}^{N_p} \sigma_{k,i}^2 = g_k$ , and  $g_k$  represents the path gain of user  $k$ . The path gains  $g_k$ 's are uniformly generated between -10 dB and 10 dB, the number of paths for each user is set  $N_p = 8$  and further assume different path signals are uncorrelated. For the COST 2100 channel model, same with [22], we consider three scattering clusters which are randomly located within the angular range  $[-1, 1)$  (parameterized by  $\xi = \frac{\sin \theta}{\sin \theta_{\max}}$ , where  $\theta \in [-\theta_{\max}, \theta_{\max})$  is the AoD). The angular interval sizes corresponding to three scattering clusters are all set 0.2. The channel angular scattering function (ASF) for each user is obtained by selecting randomly from two out of three such clusters and the ASF is nonzero over the intervals corresponding to the selected clusters and zero elsewhere.

We consider  $M = 64$  antennas  $S = 8$  RF chains. For the comparison with the original version of ACS in [22], we also plot the performance of RCSHP and ACS with unlimited RF chains, denoted by 'RCSHP-free' and 'ACS-free', respectively. Also note that the ranks of channel covariance matrix generated from the geometry-based channel model and COST 2100 channel model in this setting are 8 and (roughly) 36, respectively. This indicates in our simulations the geometry-based channel model is relatively sparse and COST 2100 channel model is less sparse. The transmit power budget at the BS is set  $P_{\max} = 10$  dB, the number of time-sharing factors is  $L = 4$  and each coherence time of channel statistics consists of 200 time slots. We consider performance in one coherence time of channel statistics for simplicity. As such, all results of the following performance comparison, i.e., sum rate, proportional fairness (PFS) utility and normalized channel estimation error, are averaged over 200 time slots. For both RCSHP and THP, the number of new channel realizations and new channel estimation noise realizations at each iteration is set  $T_{HN} = 9$  and the maximum number of iteration is 100. This two parameters can be flexibly adjusted according to the practical needs.

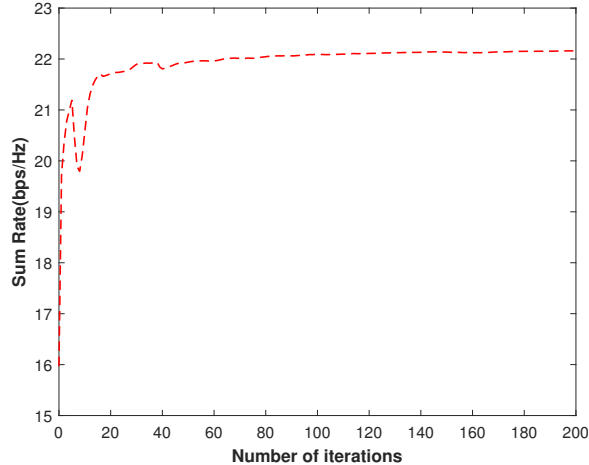


**Fig. 5:** Convergence of SSCA-RCSHP.

#### A. Convergence of the proposed SSCA-RCSHP

We use the sum rate maximization in the geometry-based channel model to illustrate the convergence of SSCA-RCSHP. Specifically, the assigned number of pilot is set  $T_p = 8$  and the number of user is  $K = 8$ . To show the convergence more clear, we set the number of iteration 200. Fig. 5 plots the sum rate versus the number of iteration, which can be seen that the proposed SSCA-RCSHP can converge to a KKT point within about 50 iterations.

#### B. Sum Rate Maximization

Fig. 6a and Fig. 6b show the sum rate versus the number of pilot in the COST 2100 channel and geometry-based channel, respectively. Each time slot contains  $T = 64$  symbols and consider  $K = 8$  users. The proposed RCSHP achieves better performance than ACS and THP. Moreover, we can observe that the performance gap between RCSHP and ACS is larger in the relatively sparse geometry-based channel, since ACS can not fully exploit beamforming gain when the channel is sparse. While RCSHP is a general utility optimization-based scheme, it can achieve a better beamforming gain in sparse channels. Further, it can be seen that RCSHP can achieve significantly better performance when the number of pilot is small, which indicates RCSHP can sparsify channels more "efficiently" and will perform better compared with ACS and THP when channel changes relatively fast, i.e., the size of each time slot  $T$  is relatively small. Fig. 7a and Fig. 7b plot the sum rate versus the number of pilot in the COST 2100 channel and

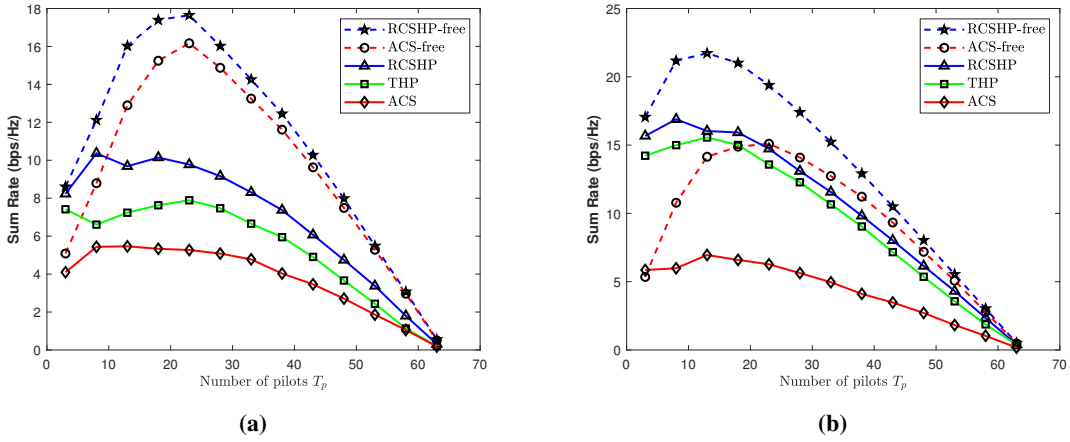


**Fig. 6:** (a) Sum rate versus the number of pilot in the COST 2100 channel ( $T = 64$ ). (b) Sum rate versus the number of pilot in the geometry-based channel ( $T = 64$ ).

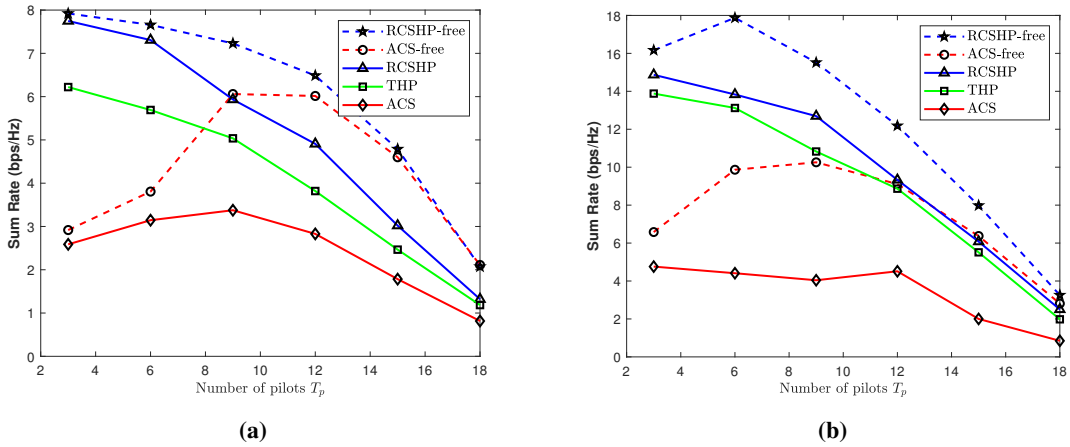


**Fig. 7:** (a) Sum rate versus the number of pilot in the COST 2100 channel ( $T = 20$ ). (b) Sum rate versus the number of pilot in the geometry-based channel ( $T = 20$ ).

geometry-based channel when setting time slot size  $T = 20$ , respectively. It can be seen that the performance gap becomes larger.

### C. Proportional Fairness

In Fig. 8a and Fig. 8b, we plot the PFS utility versus the number of pilot in the COST 2100 channel and geometry-based channel, respectively. The size of each time slot is set  $T = 64$  and the number of user is  $K = 12$ . Similar results to Fig. 6a and Fig. 6b can be observed. The results

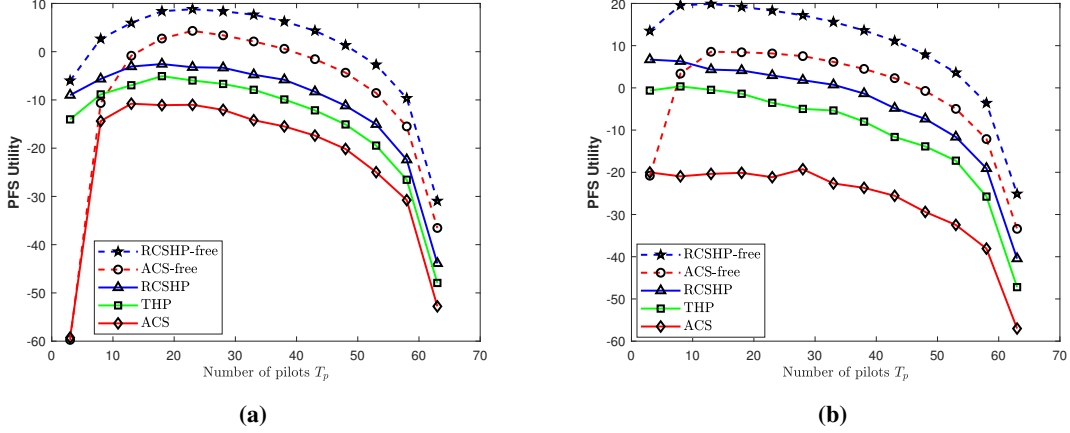


**Fig. 8:** (a) PFS utility versus the number of pilot in the COST 2100 channel ( $T = 64$ ). (b) PFS utility versus the number of pilot in the geometry-based channel ( $T = 64$ ).

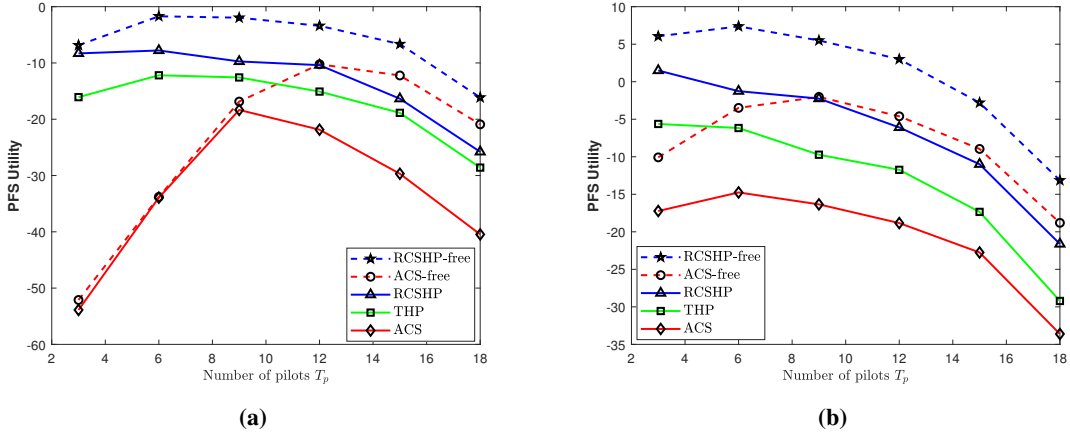


**Fig. 9:** (a) PFS utility versus the number of pilot in the COST 2100 channel ( $T = 20$ ). (b) PFS utility versus the number of pilot in the geometry-based channel ( $T = 20$ ).

of fast channel, i.e., time slot size  $T = 20$ , are also showed in Fig. 9a and Fig. 9b. Note that the performance gap between RCSHP and ACS is tremendously large when the assigned number of pilot is  $T_p = 3$ , since without considering the fairness, the minimum data rate of users becomes much smaller when the assigned number of pilot is small.

## VII. CONCLUSION

We propose a novel RCSHP design for FDD massive MIMO systems. RCSHP formulates the design as a joint optimization of the randomized control policy, i.e., the time-sharing factors

and the associated sets of analog precoders and power allocations. Specifically, at the beginning of each coherence time of channel statistics, we solve a general utility optimization over the randomized control policy by using the proposed SSCA-RCSHP algorithm with the knowledge of channel covariances (channel statistics information) of users. Then we apply the optimized randomized control policy to the current coherence time of channel statistics. At each time slot, the BS only needs to estimate the effective CSI of scheduled users to exploit the spatial multiplexing gain using a duality-based digital precoder. Such a RCSHP design can automatically group users such that in each user group, the (effective) CSI is sparse enough to be well estimated using limited pilot resource and also has enough spatial DoF to support simultaneous transmission to these users. Moreover, simulations show that RCSHP achieve a larger performance gain over the state-of-the-art ACS method specially when the number of assigned pilots is small and the channel is sparse.

## APPENDIX A

### JACOBIAN MATRIX OF INSTANTANEOUS RATE

First we define some useful notations:  $\mathbf{I}_N$  denotes a  $N \times N$  identity matrix.  $\mathbf{E}_{ii} \in \mathbb{R}^{K \times K}$  is a matrix whose  $(i, i)$ -th element is one and all other elements are zero.  $\mathbf{E}_i^{T_p} \in \mathbb{R}^{KT_p \times T_p}$  is a matrix whose  $(i-1)T_p + 1$ -th row to  $iT_p$ -th row is stacked into an identity matrix  $\mathbf{I}_{T_p}$ . Similarly,  $\mathbf{E}_{ii}^{T_p} \in \mathbb{R}^{KT_p \times KT_p}$  is a matrix whose  $(i-1)T_p + 1$ -th row to  $iT_p$ -th row and  $(i-1)T_p + 1$ -th column to  $iT_p$ -th column is put into an identity matrix  $\mathbf{I}_{T_p}$ .  $\mathbf{E}_i^M \in \mathbb{R}^{KM \times M}$  is a matrix whose  $(i-1)M + 1$ -th row to  $iM$ -th row is put into an identity matrix  $\mathbf{I}_M$ . Define an aggregated covariance matrix  $\mathbf{C} = [\mathbf{C}_1, \dots, \mathbf{C}_K] \in \mathbb{C}^{M \times KM}$ , we have

$$\begin{aligned} \mathbf{A} &= \mathbf{F}^H \mathbf{C} (\mathbf{I}_K \otimes \mathbf{F} \Psi^H), \\ \mathbf{B} &= \sum_{i=1}^K \mathbf{E}_i^{T_p} (\Psi \mathbf{A} + \mathbf{1}_K^T \otimes \mathbf{I}_{T_p}) \mathbf{E}_{ii}^{T_p}, \\ \mathbf{Y} &= \sum_{i=1}^K \mathbf{E}_i^{T_p} (\mathbf{H} \mathbf{F} \Psi^H)^H \mathbf{E}_{ii}, \\ \hat{\mathbf{G}} &= \sum_{i=1}^K \mathbf{E}_i^M \bar{\mathbf{G}} \mathbf{E}_{ii}, \end{aligned}$$

where  $\mathbf{1}_K \in \mathbb{R}^{K \times 1}$  is an all-one vector. Furthermore, define  $(\mathbf{Z}_{mn})_{\text{Blk}}$  and  $(\mathbf{Z}_{nm})_{\text{Blk}}$  to represent a block matrix whose  $(m, n)$ -th block is matrix  $\mathbf{Z}_{mn}$  and matrix  $\mathbf{Z}_{nm}$ , respectively, where  $m =$

$1, \dots, M$  and  $n = 1, \dots, S$ , and  $(\mathbf{Z})_{\text{Blk}}$  denotes a block matrix whose all  $M \times S$  blocks are matrix  $\mathbf{Z}$ . Then denote  $\mathbf{J}_{mn} \in \mathbb{R}^{M \times S}$  is a matrix whose  $(m, n)$ -th element is one and all other elements are zero, and  $\bar{\mathbf{J}}_{nm} = \mathbf{J}_{mn}^T$ . Then we have  $\bar{\mathbf{E}} = (\mathbf{J}_{mn})_{\text{Blk}} \in \mathbb{R}^{M^2 \times S^2}$ ,  $\bar{\mathbf{F}} = (\mathbf{F})_{\text{Blk}} \in \mathbb{C}^{M^2 \times S^2}$ ,  $\bar{\mathbf{E}}_h = (\bar{\mathbf{J}}_{nm})_{\text{Blk}} \in \mathbb{R}^{MS \times MS}$ ,  $\bar{\mathbf{F}}_h = (\mathbf{F}^H)_{\text{Blk}} \in \mathbb{C}^{MS \times MS}$ ,  $\tilde{\mathbf{F}} = (\mathbf{I}_K \otimes \sqrt{-1} [\mathbf{F}]_{mn} \mathbf{J}_{mn})_{\text{Blk}} \in \mathbb{C}^{KM^2 \times KS^2}$  and  $\tilde{\mathbf{F}}_h = (\mathbf{I}_K \otimes -\sqrt{-1} [\mathbf{F}]_{mn}^* \bar{\mathbf{J}}_{nm})_{\text{Blk}} \in \mathbb{C}^{KMS \times KMS}$ . Then we introduce some notations:

$$\begin{aligned} \bar{\mathbf{A}} &= -\sqrt{-1} (\bar{\mathbf{F}}_h \circ \bar{\mathbf{E}}_h) (\mathbf{I}_S \otimes \mathbf{C} (\mathbf{I}_K \otimes \mathbf{F} \Psi^H)) \\ &\quad + (\mathbf{I}_M \otimes \mathbf{F}^H \mathbf{C}) \tilde{\mathbf{F}} (\mathbf{I}_{SK} \otimes \Psi^H), \\ \bar{\mathbf{H}}_h &= \bar{\mathbf{A}} (\mathbf{I}_S \otimes \mathbf{B}^{-1} \mathbf{Y}) + \sum_{i=1}^K \left( \mathbf{I}_M \otimes \mathbf{A} \mathbf{B}^{-1} \mathbf{E}_i^{T_p} \Psi \right) \\ &\quad \left( -\sqrt{-1} (\bar{\mathbf{F}}_h \circ \bar{\mathbf{E}}_h) (\mathbf{I}_S \otimes \mathbf{H}^H \mathbf{E}_{ii}) - \bar{\mathbf{A}} (\mathbf{I}_S \otimes \mathbf{E}_{ii}^{T_p} \mathbf{B}^{-1} \mathbf{Y}) \right), \\ \bar{\mathbf{A}}_h &= (\mathbf{I}_{MK} \otimes \Psi) \tilde{\mathbf{F}}_h (\mathbf{I}_S \otimes \mathbf{C}^H \mathbf{F}) \\ &\quad + (\mathbf{I}_M \otimes (\mathbf{I}_K \otimes \Psi \mathbf{F}^H) \mathbf{C}^H) \sqrt{-1} (\bar{\mathbf{F}} \circ \bar{\mathbf{E}}), \\ \bar{\mathbf{H}} &= \left( \mathbf{I}_M \otimes (\mathbf{B}^{-1} \mathbf{Y})^H \right) \bar{\mathbf{A}}_h \\ &\quad + \sum_{i=1}^K \left( \sqrt{-1} (\mathbf{I}_M \otimes \mathbf{E}_{ii} \mathbf{H}) (\bar{\mathbf{F}} \circ \bar{\mathbf{E}}) - \right. \\ &\quad \left. \left( \mathbf{I}_M \otimes (\mathbf{B}^{-1} \mathbf{Y})^H \mathbf{E}_{ii}^{T_p} \right) \bar{\mathbf{A}}_h \right) \left( \mathbf{I}_S \otimes \left( \mathbf{A} \mathbf{B}^{-1} \mathbf{E}_i^{T_p} \Psi \right)^H \right). \end{aligned}$$

Further, define  $\mathbf{V} = \hat{\mathbf{H}}^H \hat{\mathbf{P}} \hat{\mathbf{H}} + \mathbf{I}$  and  $\tilde{\mathbf{G}} = \mathbf{V}^{-1} \hat{\mathbf{H}}^H \hat{\mathbf{P}}$ , we have

$$\begin{aligned} \bar{\mathbf{D}} &= (\mathbf{I}_M \otimes \mathbf{F} \mathbf{V}^{-1}) \bar{\mathbf{H}}_h \left( \mathbf{I}_S \otimes \left( \mathbf{P} - \hat{\mathbf{P}} \hat{\mathbf{H}} \tilde{\mathbf{G}} \right) \right) \\ &\quad + \left( \sqrt{-1} (\bar{\mathbf{F}} \circ \bar{\mathbf{E}}) - (\mathbf{I}_M \otimes \tilde{\mathbf{G}}) \bar{\mathbf{H}} \right) \left( \mathbf{I}_S \otimes \tilde{\mathbf{G}} \right), \\ \bar{\mathbf{D}}_h &= \left( \mathbf{I}_M \otimes \left( \mathbf{P} - \hat{\mathbf{P}} \hat{\mathbf{H}} \tilde{\mathbf{G}} \right) \right) \bar{\mathbf{H}} (\mathbf{I}_S \otimes \mathbf{V}^{-1} \mathbf{F}^H) \\ &\quad - \left( \mathbf{I}_M \otimes \tilde{\mathbf{G}}^H \right) \left( \sqrt{-1} (\bar{\mathbf{F}}_h \circ \bar{\mathbf{E}}_h) + \bar{\mathbf{H}}_h (\mathbf{I}_S \otimes \tilde{\mathbf{G}}^H) \right), \\ \mathbf{A}_F &= \sum_{i=1}^K - (\mathbf{I}_M \otimes \Lambda \mathbf{E}_{ii}) \bar{\mathbf{D}}_h \left( \mathbf{I}_S \otimes \frac{1}{2} \left( \Lambda^{\frac{1}{2}} \hat{\mathbf{G}}^H \mathbf{E}_i^M \right)^H \right) \\ &\quad - \left( \mathbf{I}_M \otimes \Lambda \hat{\mathbf{G}}^H \mathbf{E}_i^M \right) \bar{\mathbf{D}} \left( \mathbf{I}_S \otimes \frac{1}{2} \mathbf{E}_{ii} \Lambda^{\frac{1}{2}} \right), \\ \mathbf{G}_F &= (\mathbf{I}_M \otimes \mathbf{V}^{-1}) \bar{\mathbf{H}}_h \left( \mathbf{I}_S \otimes \left( \mathbf{P} \Lambda^{\frac{1}{2}} - \hat{\mathbf{P}} \hat{\mathbf{H}} \tilde{\mathbf{G}} \right) \right) \\ &\quad + \left( \mathbf{I}_M \otimes \tilde{\mathbf{G}} \right) \left( \mathbf{A}_F - \bar{\mathbf{H}} (\mathbf{I}_S \otimes \tilde{\mathbf{G}}) \right). \end{aligned}$$

According to the matrix calculus, the gradient of instantaneous data rate  $r_k(\boldsymbol{\theta}(l), \mathbf{p}(l); \mathbf{H}, \mathbf{N}, l)$  w.r.t.  $\boldsymbol{\theta}(l)$  is given by

$$\nabla_{\boldsymbol{\theta}(l)} r_k = \frac{\sum_{i=1}^K \mathbf{a}_{k,i}^{\theta_l}}{\Gamma_k} - \frac{\sum_{i \neq k} \mathbf{a}_{k,i}^{\theta_l}}{\Gamma_{-k}}, \quad (22)$$

where  $\Gamma_k = \sum_{i=1}^K p_i |\mathbf{h}_k^H \mathbf{F} \mathbf{g}_i|^2 + 1$ ,  $\Gamma_{-k} = \sum_{i \neq k} p_i |\mathbf{h}_k^H \mathbf{F} \mathbf{g}_i|^2 + 1$ ,

$$\mathbf{a}_{k,i}^{\theta_l} = \text{Vec} \left\{ 2p_i \Re \left[ [\mathbf{HFG}]_{ki}^* \left( (\mathbf{I}_M \otimes [\mathbf{H}]_{k.}) (\sqrt{-1} \bar{\mathbf{F}} \circ \bar{\mathbf{E}}) \right. \right. \right. \\ \left. \left. \left. (\mathbf{I}_S \otimes [\mathbf{G}]_{.i}) + (\mathbf{I}_M \otimes [\mathbf{HF}]_{k.}) \mathbf{G}_F (\mathbf{I}_S \otimes \mathbf{e}_i) \right) \right] \right\},$$

$\mathbf{e}_i \in \mathbb{R}^{K \times 1}$  is a vector whose  $i$ -th element is one and all other elements are zero.

Note that we have omitted the control state  $l$  and  $(\boldsymbol{\theta}(l), \mathbf{p}(l); \mathbf{H}, \mathbf{N}, l)$  in the gradient expression for simplicity, and we also keep this habit for the gradient of  $r_k(\boldsymbol{\theta}(l), \mathbf{p}(l); \mathbf{H}, \mathbf{N}, l)$  over  $\mathbf{p}(l)$ .  $\bar{\mathbf{P}} \in \mathbb{R}^{K^2 \times K}$  is a matrix whose  $(i-1)K+1$ -th row to  $iK$ -th row is put into  $\mathbf{E}_{ii}$ , where  $i = 1, \dots, K$ . Then we introduce some notations:

$$\begin{aligned} \bar{\mathbf{D}}_p &= \left( \bar{\mathbf{P}} - \left( \mathbf{I}_K \otimes \left( \hat{\mathbf{H}} \tilde{\mathbf{G}} \right)^H \right) \bar{\mathbf{P}} \right) \hat{\mathbf{H}} \mathbf{V}^{-1} \mathbf{F}^H, \\ \mathbf{D}_p &= \left( \mathbf{I}_K \otimes \mathbf{F} \mathbf{V}^{-1} \hat{\mathbf{H}} \right) \left( \bar{\mathbf{P}} - \bar{\mathbf{P}} \hat{\mathbf{H}} \tilde{\mathbf{G}} \right), \\ \mathbf{A}_p &= \sum_{i=1}^K -\frac{1}{2} \left( \mathbf{I}_K \otimes \Lambda \mathbf{E}_{ii} \right) \bar{\mathbf{D}}_p \left( \hat{\mathbf{G}}^H \mathbf{E}_i^M \right)^H \Lambda^{\frac{1}{2}} \\ &\quad - \frac{1}{2} \left( \mathbf{I}_K \otimes \Lambda \hat{\mathbf{G}}^H \mathbf{E}_i^M \right) \mathbf{D}_p \mathbf{E}_{ii} \Lambda^{\frac{1}{2}}, \\ \mathbf{G}_p &= \left( \mathbf{I}_K \otimes \mathbf{V}^{-1} \hat{\mathbf{H}} \right) \bar{\mathbf{P}} \left( \Lambda^{\frac{1}{2}} - \hat{\mathbf{H}} \tilde{\mathbf{G}} \right) + \left( \mathbf{I}_K \otimes \tilde{\mathbf{G}} \right) \mathbf{A}_p. \end{aligned}$$

Thus using matrix calculus, the gradient of instantaneous data rate  $r_k(\boldsymbol{\theta}(l), \mathbf{p}(l); \mathbf{H}, \mathbf{N}, l)$  w.r.t  $\mathbf{p}(l)$  is given by

$$\nabla_{\mathbf{p}(l)} r_k = \frac{\sum_{i=1}^K \mathbf{a}_{k,i}^{p_l}}{\Gamma_k} - \frac{\sum_{i \neq k} \mathbf{a}_{k,i}^{p_l}}{\Gamma_{-k}}, \quad (24)$$

where

$$\begin{aligned} \mathbf{a}_{k,i}^{p_l} &= 2p_i \Re \left[ [\mathbf{HFG}]_{ki}^* \left( \mathbf{I}_K \otimes [\mathbf{HF}]_{k.} \right) [\mathbf{G}_p]_{.i} \right] \\ &\quad + \mathbf{e}_i |[\mathbf{HFG}]_{ki}|^2. \end{aligned}$$

Therefore, for given channel state  $\mathbf{H}$  and channel estimation noise state  $\mathbf{N}$ , the Jacobian matrix of the data rate vector  $\tilde{\mathbf{r}}(\mathbf{\Gamma}, \mathbf{q}; \mathbf{H}, \mathbf{N})$  w.r.t.  $\mathbf{\Gamma}$  is

$$\mathbf{J}_{\mathbf{\Gamma}}(\mathbf{\Gamma}, \mathbf{q}; \mathbf{H}, \mathbf{N}) = \begin{bmatrix} q_1 \nabla_{\boldsymbol{\theta}(1)} r_1 & \cdots & q_1 \nabla_{\boldsymbol{\theta}(1)} r_K \\ q_1 \nabla_{\mathbf{p}(1)} r_1 & \cdots & q_1 \nabla_{\mathbf{p}(1)} r_K \\ \vdots & & \vdots \\ q_L \nabla_{\boldsymbol{\theta}(L)} r_1 & \cdots & q_L \nabla_{\boldsymbol{\theta}(L)} r_K \\ q_L \nabla_{\mathbf{p}(L)} r_1 & \cdots & q_L \nabla_{\mathbf{p}(L)} r_K \end{bmatrix}. \quad (25)$$

## APPENDIX B

### PROOF OF LEMMA 1

The proof relies on the following lemma.

**Lemma 2.** Define  $\check{r}_k^t(l) = \mathbb{E}_{\mathbf{H}, \mathbf{N}} [r_k(\mathbf{\Gamma}^t(l); \mathbf{H}, \mathbf{N}, l)]$ , then under Assumption 1, we have

$$\lim_{t \rightarrow \infty} |\hat{r}_k^t(l) - \check{r}_k^t(l)| = 0, \forall k, \forall l, \quad (26)$$

$$\lim_{t \rightarrow \infty} \|\mathbf{f}_{\mathbf{\Gamma}}^t - \nabla_{\mathbf{\Gamma}} f(\mathbf{\Gamma}^t, \mathbf{q}^t)\| = 0. \quad (27)$$

*Proof.* For (26), it is a consequence of [35], Lemma 1. It is easy to verify that the technical conditions (a), (b), (c) and (d) therein are satisfied. Moreover, it follows from the Lipschitz continuity of  $r_k(\mathbf{\Gamma}^t(l); \mathbf{H}, \mathbf{N}, l)$  that

$$\begin{aligned} \lim_{t \rightarrow \infty} \frac{|\check{r}_k^{t+1}(l) - \check{r}_k^t(l)|}{\rho_t} &\leq \lim_{t \rightarrow \infty} \frac{L_{\mathbf{\Gamma}} \|\mathbf{\Gamma}^{t+1}(l) - \mathbf{\Gamma}^t(l)\|}{\rho_t} \\ &= \lim_{t \rightarrow \infty} O\left(\frac{\gamma_t}{\rho_t}\right) = 0, \end{aligned}$$

where  $L_{\mathbf{\Gamma}}$  is the Lipschitz constant. Therefore, the technical condition (e) in [35] is also satisfied and (26) is proved.

The proof of (27) consists of two steps. For the consideration of simplicity, let  $\bar{\mathbf{r}}^t = \bar{\mathbf{r}}(\mathbf{\Gamma}^t, \mathbf{q}^t)$ ,  $\hat{\mathbf{r}}^t = \hat{\mathbf{r}}^t(\mathbf{q}^t)$  and  $\nabla_{\mathbf{\Gamma}}^t f = \nabla_{\mathbf{\Gamma}} f(\mathbf{\Gamma}^t, \mathbf{q}^t)$ .

*Step 1 of proving (27):* Define a sequence

$$\check{r}_k^t = \sum_{l=1}^L q_l^t \sum_{i=1}^t r_k(\mathbf{\Gamma}^t(l); \mathbf{H}(i), \mathbf{N}(i), l), \forall k. \quad (28)$$

Denote  $\tilde{\mathbf{r}}^t = [\tilde{r}_1^t, \dots, \tilde{r}_K^t]^\top$ . According to the law of large numbers, the central limit theorem and the Berry-Esseen theorem, we have  $\lim_{t \rightarrow \infty} \|\tilde{\mathbf{r}}^t - \bar{\mathbf{r}}^t\| = 0$  and  $\mathbb{E} \|\tilde{\mathbf{r}}^t - \bar{\mathbf{r}}^t\| = O\left(\frac{1}{\sqrt{t}}\right)$ . Further we define a sequence

$$\begin{aligned} \hat{\mathbf{f}}_\Gamma^t &= (1 - \rho_t) \hat{\mathbf{f}}_\Gamma^{t-1} \\ &+ \rho_t \sum_{i=1}^{T_{HN}} \frac{\mathbf{J}_\Gamma(\Gamma^t, \mathbf{q}^t; \mathbf{H}^t(i), \mathbf{N}^t(i)) \nabla_{\bar{\mathbf{r}}} U(\tilde{\mathbf{r}}^t)}{T_{HN}}. \end{aligned} \quad (29)$$

It can be seen that the update term in (29), which is denoted by  $\tilde{\mathbf{f}}_\Gamma^t$ , is only different from (13)

$$\text{by } e_t = \left| \sum_{i=1}^{T_{HN}} \frac{\mathbf{J}_\Gamma(\Gamma^t, \mathbf{q}^t; \mathbf{H}^t(i), \mathbf{N}^t(i)) \left( \nabla_{\bar{\mathbf{r}}} U(\tilde{\mathbf{r}}^t) - \nabla_{\bar{\mathbf{r}}} U(\hat{\mathbf{r}}^t) \right)}{T_{HN}} \right|.$$

Further we have

$$\lim_{t \rightarrow \infty} \left\| \hat{\mathbf{f}}_\Gamma^t - \nabla_{\bar{\mathbf{r}}}^t f \right\| = 0. \quad (30)$$

This is a consequence of [35], Lemma 1. It is easy to verify that the technical conditions (a), (b), (d) and (e) in [35], Lemma 1 are satisfied. Moreover, follow from that  $\nabla_{\bar{\mathbf{r}}} U$  is Lipschitz continuous and  $\mathbf{J}_\Gamma^t$  is bounded w.p.1., we have

$$\begin{aligned} \left\| \mathbb{E} \left[ \tilde{\mathbf{f}}_\Gamma^t \right] - \nabla_{\bar{\mathbf{r}}}^t f \right\| &\leq \mathbb{E} \left\| \mathbf{J}_\Gamma^t \left( \nabla_{\bar{\mathbf{r}}} U(\tilde{\mathbf{r}}^t) - \nabla_{\bar{\mathbf{r}}} U(\bar{\mathbf{r}}^t) \right) \right\| \\ &= O\left(\|\tilde{\mathbf{r}}^t - \bar{\mathbf{r}}^t\|\right) = O\left(\frac{1}{\sqrt{t}}\right). \end{aligned} \quad (31)$$

From Assumption 1-1), we have  $\sum_t \rho_t \left\| \mathbb{E} \left[ \tilde{\mathbf{f}}_\Gamma^t \right] - \nabla_{\bar{\mathbf{r}}}^t f \right\| < \infty$ , which implies the technical condition (c) in [35], Lemma 1 is satisfied.

*Step 2 of proving (27):* From the definitions of  $\hat{\mathbf{f}}_\Gamma^t$  and  $\mathbf{f}_\Gamma^t$ , we have

$$\begin{aligned} &\left\| \hat{\mathbf{f}}_\Gamma^t - \mathbf{f}_\Gamma^t \right\| \\ &\leq \sum_{t'=1}^t (1 - \rho_t)^{t-t'} \rho_{t'} e_{t'} \\ &= \sum_{t'=1}^{n_t} (1 - \rho_t)^{t-t'} \rho_{t'} e_{t'} + \sum_{t'=n_t+1}^t (1 - \rho_t)^{t-t'} \rho_{t'} e_{t'} \\ &\leq \rho_1 e_{t_a} \frac{(1 - \rho_t)^{t-n_t}}{\rho_t} + \frac{\rho_{n_t+1}}{\rho_t} e_{t_b}, \end{aligned} \quad (32)$$

where  $n_t = (1 - \beta - \epsilon)t$  with  $\epsilon \in (0, 1 - \beta)$ ,  $e_{t_a} = \max_{t' \in \{1, \dots, n_t\}} e_{t'}$  and  $e_{t_b} = \max_{t' \in \{n_t+1, \dots, t\}} e_{t'}$ .

From Assumption 1-1), we have  $\lim_{t \rightarrow \infty} \rho_1 e_{t_a} \frac{(1 - \rho_t)^{t-n_t}}{\rho_t} = 0$  and  $\frac{\rho_{n_t+1}}{\rho_t} < \infty$ . Then it follows from the above analysis that

$$\lim_{t \rightarrow \infty} \left\| \hat{\mathbf{f}}_\Gamma^t - \mathbf{f}_\Gamma^t \right\| = \lim_{t_b \rightarrow \infty} O(e_{t_b}) \stackrel{a}{=} \lim_{t_b \rightarrow \infty} O\left(\left\| \tilde{\mathbf{r}}^{t_b} - \hat{\mathbf{r}}^{t_b} \right\|\right) \stackrel{b}{=} 0, \quad (33)$$

where (33)-a holds because  $\nabla_{\bar{\mathbf{r}}}U$  is Lipschitz continuous and  $\mathbf{J}_{\Gamma}^t$  is bounded w.p.1., and (33)-b holds because  $\lim_{t \rightarrow \infty} \|\hat{\bar{\mathbf{r}}^t} - \bar{\mathbf{r}}^t\| = 0$  and  $\lim_{t \rightarrow \infty} \|\check{\mathbf{r}}^t - \bar{\mathbf{r}}^t\| = 0$ . Together with (30), it follows that (27) holds.  $\square$

From Lemma 2, we can immediately have that  $\bar{f}^{t_j}(\Gamma, \mathbf{q})$  converges to  $\hat{f}(\Gamma, \mathbf{q})$  almost surely. This completes the proof.

## APPENDIX C

### PROOF OF THEOREM 1

Denote  $\phi = [\Gamma^T, \mathbf{q}^T]^T$  as the composite variable and  $\bar{\phi} = [\bar{\Gamma}^T, \bar{\mathbf{q}}^T]^T$  as the optimal solution of the surrogate problem (14), respectively. Then we simply define  $f(\Gamma, \mathbf{q})$  as  $f(\phi)$  and  $\bar{f}^t(\Gamma, \mathbf{q})$  as  $\bar{f}^t(\phi)$ , respectively. The proof of Theorem 1 can be split into three steps.

1. We first prove that  $\liminf_{t \rightarrow \infty} \|\bar{\phi}^t - \phi^t\| = 0$  w.p.1.

Since  $\bar{f}^t(\phi)$  is strongly concave over  $\phi$ , we have

$$\nabla_{\phi}^T \bar{f}^t(\phi^t) \mathbf{d}^t \geq \eta \|\mathbf{d}^t\|^2 + \bar{f}^t(\bar{\phi}^t) - \bar{f}^t(\phi^t) \geq \eta \|\mathbf{d}^t\|^2 \quad (34)$$

for some  $\eta > 0$ , where  $\mathbf{d}^t = \bar{\phi}^t - \phi^t$ . Moreover, the gradient  $\nabla_{\phi} f(\phi)$  is Lipschitz continuous, and thus there exists a constant  $L_0 > 0$  such that

$$\begin{aligned} f(\phi^{t+1}) &\geq f(\phi^t) + \gamma_t \nabla_{\phi}^T f(\phi^t) \mathbf{d}^t - L_0 (\gamma_t)^2 \|\mathbf{d}^t\|^2 \\ &= f(\phi^t) - L_0 (\gamma_t)^2 \|\mathbf{d}^t\|^2 \\ &\quad + \gamma_t (\nabla_{\phi}^T f(\phi^t) - \nabla_{\phi}^T \bar{f}^t(\phi^t) + \nabla_{\phi}^T \bar{f}^t(\phi^t)) \mathbf{d}^t \\ &\geq f(\phi^t) + \gamma_t \eta \|\mathbf{d}^t\|^2 - o(\gamma_t), \end{aligned}$$

where the last inequality follows from equation (34) and  $\lim_{t \rightarrow \infty} \|\nabla_{\phi} f(\phi^t) - \nabla_{\phi} \bar{f}^t(\phi^t)\| = 0$ , which is a result of Lemma 1. Next, we show by contradiction that  $\liminf_{t \rightarrow \infty} \|\bar{\phi}^t - \phi^t\| = 0$  w.p.1. Suppose  $\liminf_{t \rightarrow \infty} \|\bar{\phi}^t - \phi^t\| \geq \chi > 0$  with a positive probability. Then we can find a realization such that  $\|\mathbf{d}^t\| \geq \chi, \forall t$ . We focus on such a realization. By choosing a sufficient large  $t_0$ , then there exists a constant  $\bar{\eta} > 0$ , such that

$$f(\phi^{t+1}) - f(\phi^t) \geq \gamma_t \bar{\eta} \|\mathbf{d}^t\|^2, \forall t \geq t_0. \quad (35)$$

Then it follows from (35) that

$$f(\phi^t) - f(\phi^{t_0}) \geq \bar{\eta} \chi^2 \sum_{j=t_0}^{t-1} \gamma_j,$$

which, in view of  $\sum_{j=t_0}^{\infty} \gamma_j = \infty$ , contradicts the boundness of  $\{f(\phi^t)\}$ . Therefore, it must be  $\liminf_{t \rightarrow \infty} \|\bar{\phi}^t - \phi^t\| = 0$  w.p.1.

2. Then we prove that  $\limsup_{t \rightarrow \infty} \|\bar{\phi}^t - \phi^t\| = 0$  w.p.1.

We first prove a useful lemma.

**Lemma 3.** *There exists a constant  $L > 0$  such that*

$$\|\bar{\phi}^{t_1} - \bar{\phi}^{t_2}\| \leq L \|\phi^{t_1} - \phi^{t_2}\| + e(t_1, t_2),$$

where  $\lim_{t_1, t_2 \rightarrow \infty} e(t_1, t_2) = 0$ .

From Lemma 2 and the Lipschitz continuity of  $f(\phi)$ , we have

$$|\bar{f}^{t_1}(\phi) - \bar{f}^{t_2}(\phi)| \leq C \|\phi^{t_1} - \phi^{t_2}\| + e'(t_1, t_2), \quad (36)$$

where  $\lim_{t_1, t_2 \rightarrow \infty} e'(t_1, t_2) = 0$  and  $C > 0$  is a constant. Obviously, the problem (14) is strictly convex, when the objective function is changed by some amount  $e(\phi)$ , the optimal solution  $\bar{\phi}^t$  will be changed by the same order, i.e., the change is within the range  $\pm O(|e(\phi)|)$ . Thus it follows from (36) and the strong convexity of  $\bar{f}^t(\phi)$  that

$$\|\bar{\phi}^{t_1} - \bar{\phi}^{t_2}\| \leq C_1 C \|\phi^{t_1} - \phi^{t_2}\| + C_1 e'(t_1, t_2) \quad (37)$$

for some constant  $C_1 > 0$ . Finally, Lemma 3 follows from (37) immediately.

Using Lemma 3 and the fact that  $\liminf_{t \rightarrow \infty} \|\bar{\phi}^t - \phi^t\| = 0$  w.p.1., and following the same analysis as that in [34], Proof of Theorem 1, it can be shown that  $\limsup_{t \rightarrow \infty} \|\bar{\phi}^t - \phi^t\| = 0$  w.p.1. Therefore, we have

$$\lim_{t \rightarrow \infty} \|\bar{\phi}^t - \phi^t\| = 0, \text{ w. p. 1.} \quad (38)$$

3. We are finally ready for the proof of Theorem 1.

According to Lemma 1 and equation (38), the limiting point  $\{\Gamma^*, \mathbf{q}^*\}$  is the optimal solution of the following convex problem almost surely:

$$\max_{\Gamma \in \mathcal{G}, \mathbf{q} \in \mathcal{Q}} \hat{f}(\Gamma, \mathbf{q}) \quad (39a)$$

$$\text{s.t. } \mathbf{1}^T \mathbf{p}(l) \leq P_{\max} \quad l = 1, \dots, L. \quad (39b)$$

Thus the limiting point  $\{\Gamma^*, \mathbf{q}^*\}$  satisfies the KKT conditions of (39), which are also KKT conditions of the original problem (10). This completes the proof.

## REFERENCES

- [1] E. G. Larsson, O. Edfors, F. Tufvesson, and T. L. Marzetta, "Massive mimo for next generation wireless systems," *IEEE Communications Magazine*, vol. 52, no. 2, pp. 186–195, February 2014.
- [2] F. Rusek, D. Persson, B. K. Lau, E. G. Larsson, T. L. Marzetta, O. Edfors, and F. Tufvesson, "Scaling up mimo: Opportunities and challenges with very large arrays," *IEEE Signal Processing Magazine*, vol. 30, no. 1, pp. 40–60, Jan 2013.
- [3] J. Choi, D. J. Love, and P. Bidigare, "Downlink training techniques for fdd massive mimo systems: Open-loop and closed-loop training with memory," *IEEE Journal of Selected Topics in Signal Processing*, vol. 8, no. 5, pp. 802–814, Oct 2014.
- [4] Z. Gao, L. Dai, Z. Wang, and S. Chen, "Spatially common sparsity based adaptive channel estimation and feedback for fdd massive mimo," *IEEE Transactions on Signal Processing*, vol. 63, no. 23, pp. 6169–6183, Dec 2015.
- [5] H. Ji, Y. Kim, J. Lee, E. Onggosanusi, Y. Nam, J. Zhang, B. Lee, and B. Shim, "Overview of full-dimension mimo in lte-advanced pro," *IEEE Communications Magazine*, vol. 55, no. 2, pp. 176–184, February 2017.
- [6] J. Shen, J. Zhang, K. Chen, and K. B. Letaief, "High-dimensional csi acquisition in massive mimo: Sparsity-inspired approaches," *IEEE Systems Journal*, vol. 11, no. 1, pp. 32–40, March 2017.
- [7] W. U. Bajwa, J. Haupt, A. M. Sayeed, and R. Nowak, "Compressed channel sensing: A new approach to estimating sparse multipath channels," *Proceedings of the IEEE*, vol. 98, no. 6, pp. 1058–1076, June 2010.
- [8] X. Rao and V. K. N. Lau, "Distributed compressive csit estimation and feedback for fdd multi-user massive mimo systems," *IEEE Transactions on Signal Processing*, vol. 62, no. 12, pp. 3261–3271, June 2014.
- [9] V. K. N. Lau, S. Cai, and A. Liu, "Closed-loop compressive csit estimation in fdd massive mimo systems with 1 bit feedback," *IEEE Transactions on Signal Processing*, vol. 64, no. 8, pp. 2146–2155, April 2016.
- [10] A. Liu, F. Zhu, and V. K. N. Lau, "Closed-loop autonomous pilot and compressive csit feedback resource adaptation in multi-user fdd massive mimo systems," *IEEE Transactions on Signal Processing*, vol. 65, no. 1, pp. 173–183, Jan 2017.
- [11] A. Liu, V. K. N. Lau, and M. Zhao, "Stochastic successive convex optimization for two-timescale hybrid precoding in massive mimo," *IEEE Journal of Selected Topics in Signal Processing*, vol. 12, no. 3, pp. 432–444, June 2018.
- [12] F. Sahrabi and W. Yu, "Hybrid digital and analog beamforming design for large-scale antenna arrays," *IEEE Journal of Selected Topics in Signal Processing*, vol. 10, no. 3, pp. 501–513, April 2016.
- [13] X. Gao, L. Dai, S. Han, C. I, and R. W. Heath, "Energy-efficient hybrid analog and digital precoding for mmwave mimo systems with large antenna arrays," *IEEE Journal on Selected Areas in Communications*, vol. 34, no. 4, pp. 998–1009, April 2016.
- [14] X. Zhu, Z. Wang, L. Dai, and Q. Wang, "Adaptive hybrid precoding for multiuser massive mimo," *IEEE Communications Letters*, vol. 20, no. 4, pp. 776–779, April 2016.
- [15] L. Liang, W. Xu, and X. Dong, "Low-complexity hybrid precoding in massive multiuser mimo systems," *IEEE Wireless Communications Letters*, vol. 3, no. 6, pp. 653–656, Dec 2014.
- [16] A. Alkhateeb, G. Leus, and R. W. Heath, "Limited feedback hybrid precoding for multi-user millimeter wave systems," *IEEE Transactions on Wireless Communications*, vol. 14, no. 11, pp. 6481–6494, Nov 2015.
- [17] A. Liu and V. K. N. Lau, "Impact of csi knowledge on the codebook-based hybrid beamforming in massive mimo," *IEEE Transactions on Signal Processing*, vol. 64, no. 24, pp. 6545–6556, Dec 2016.
- [18] A. Adhikary, J. Nam, J. Ahn, and G. Caire, "Joint spatial division and multiplexing the large-scale array regime," *IEEE Transactions on Information Theory*, vol. 59, no. 10, pp. 6441–6463, Oct 2013.

- [19] A. Liu and V. Lau, "Phase only rf precoding for massive mimo systems with limited rf chains," *IEEE Transactions on Signal Processing*, vol. 62, no. 17, pp. 4505–4515, Sept 2014.
- [20] A. Liu and V. K. N. Lau, "Two-stage constant-envelope precoding for low-cost massive mimo systems," *IEEE Transactions on Signal Processing*, vol. 64, no. 2, pp. 485–494, Jan 2016.
- [21] S. Park, J. Park, A. Yazdan, and R. W. Heath, "Exploiting spatial channel covariance for hybrid precoding in massive mimo systems," *IEEE Transactions on Signal Processing*, vol. 65, no. 14, pp. 3818–3832, July 2017.
- [22] M. Barzegar Khalilsarai, S. Haghghatshoar, X. Yi, and G. Caire, "Fdd massive mimo via ul/dl channel covariance extrapolation and active channel sparsification," *IEEE Transactions on Wireless Communications*, vol. 18, no. 1, pp. 121–135, Jan 2019.
- [23] C. B. Peel, B. M. Hochwald, and A. L. Swindlehurst, "A vector-perturbation technique for near-capacity multiantenna multiuser communication-part i: channel inversion and regularization," *IEEE Transactions on Communications*, vol. 53, no. 1, pp. 195–202, Jan 2005.
- [24] M. Schubert and H. Boche, "Solution of the multiuser downlink beamforming problem with individual sinr constraints," *IEEE Transactions on Vehicular Technology*, vol. 53, no. 1, pp. 18–28, Jan 2004.
- [25] X. Zhang, A. F. Molisch, and S.-Y. Kung, "Variable-phase-shift-based rf-baseband codesign for mimo antenna selection," *IEEE Transactions on Signal Processing*, vol. 53, no. 11, pp. 4091–4103, Nov 2005.
- [26] S. Haghghatshoar and G. Caire, "Massive mimo channel subspace estimation from low-dimensional projections," *IEEE Transactions on Signal Processing*, vol. 65, no. 2, pp. 303–318, Jan 2017.
- [27] —, "Low-complexity massive mimo subspace estimation and tracking from low-dimensional projections," *IEEE Transactions on Signal Processing*, vol. 66, no. 7, pp. 1832–1844, April 2018.
- [28] L. Miretti, R. L. G. Cavalcante, and S. Stanczak, "Fdd massive mimo channel spatial covariance conversion using projection methods," 04 2018.
- [29] P. Viswanath and D. N. C. Tse, "Sum capacity of the vector gaussian broadcast channel and uplink-downlink duality," *IEEE Transactions on Information Theory*, vol. 49, no. 8, pp. 1912–1921, Aug 2003.
- [30] S. Wagner, R. Couillet, M. Debbah, and D. T. M. Slock, "Large system analysis of linear precoding in correlated mimo broadcast channels under limited feedback," *IEEE Transactions on Information Theory*, vol. 58, no. 7, pp. 4509–4537, July 2012.
- [31] J. Mo and J. Walrand, "Fair end-to-end window-based congestion control," *IEEE/ACM Transactions on Networking*, vol. 8, no. 5, pp. 556–567, Oct 2000.
- [32] A. Tomasoni, G. Caire, M. Ferrari, and S. Bellini, "On the selection of semi-orthogonal users for zero-forcing beamforming," in *2009 IEEE International Symposium on Information Theory*, June 2009, pp. 1100–1104.
- [33] S. Boyd and L. Vandenberghe, Eds., *Convex Optimization*. Cambridge University Press., 2004.
- [34] Y. Yang, G. Scutari, D. P. Palomar, and M. Pesavento, "A parallel decomposition method for nonconvex stochastic multi-agent optimization problems," *IEEE Transactions on Signal Processing*, vol. 64, no. 11, pp. 2949–2964, June 2016.
- [35] A. Ruszczyński, "Feasible direction methods for stochastic programming problems," *Mathematical Programming*, vol. 19, no. 1, pp. 220–229, Dec 1980. [Online]. Available: <https://doi.org/10.1007/BF01581643>